The Geological Society of America Bulletin

Stratigraphy, structure and volcano-tectonic evolution of Solfatara maar-diatreme (Campi Flegrei, Italy)

--Manuscript Draft--

Manuscript Number:	B31183R2
Full Title:	Stratigraphy, structure and volcano-tectonic evolution of Solfatara maar-diatreme (Campi Flegrei, Italy)
Short Title:	Stratigraphy, structure and volcano-tectonic evolution of Solfatara maar-diatreme (Campi Flegrei, Italy)
Article Type:	Article
Keywords:	maar-diatreme, phreatic eruptions, faults, volcano-tectonics, Electrical resistivity tomography, hydrothermal activity
Corresponding Author:	Roberto Isaia, Ph.D. Istituo Nazionale di Geofisica e Vulcanologia Napoli, Campania ITALY
Corresponding Author's Institution:	Istituo Nazionale di Geofisica e Vulcanologia
First Author:	Roberto Isaia, Ph.D.
Order of Authors:	Roberto Isaia, Ph.D.
	Stefano Vitale, Ph.D.
	Mariagiulia Di Giuseppe, Ph.D.
	Enrico Iannuzzi, Dott.
	Francesco D'Assisi Tramparulo, Ph.D.
	Antonio Troaiano, Ph.D.
Abstract:	This study focuses on the Solfatara-Pisciarelli area within the Campi Flegrei, a volcanic field located in the Tyrrhenian coast of the southern Italy. Volcanism at Campi Flegrei caldera has included phreatic to phreatomagmatic explosions, and both magmatic (ranging from small scoria producing events to those with Plinian columns) and effusive eruptions. These eruptions have formed tuff cones, tuff rings, minor scoria cones and lava domes. A detailed stratigraphic, structural and geophysical study of the area indicates that the Solfatara volcano is maar-diatreme. It is characterized by a crater cut into earlier volcanic deposits, a small rim of ejecta and a deep structure (down to 2-3 km). This maar-diatreme has allowed to the gases and fluids to flow up to the surface over a long time. A new geological map and cross sections show a complex architecture of different volcano-tectonic features including scoria cones, lavas and crypto-domes, feeder dykes, pipes, ring and regional faults, and explosive craters. Volcanological data were collected with the main aim to characterize the eruptive activity in a limited sector of the caldera. Fault and fracture analyses, using the scan line methodology, highlight the role of the main structures that accompanied the volcanic evolution within this sector of Campi Flegrei caldera. To better constrain the subsurface structure of the Solfatara crater, Electrical Resistivity Tomography (ERT) investigations were integrated with the volcano-tectonic information. All data suggest that the Solfatara area is dominated by a maar-diatreme evolution. Presently, the Solfatara-Pisciarelli area shows a widespread hydrothermal and fumarolic activity that is localized along the major faults. The results allow us to define a particular type of volcanic activity in the recent past in the area that is still considered today. It is one of the areas with a higher probability of opening new vents, particularly for possible phreatic activity.
Suggested Reviewers:	Joan Martì

	joan.marti@ija.csic.es Expert of volcano-tectonic, caldera volcanism and geophysical data apllied to volcanoes
	Guido Giordano guido.giordano@uniroma3.it Intersted and expert in maar volcanism
	Shane Cronin S.J.Cronin@massey.ac.nz Expert of phreatic and phretomagmatic eruptions and caldera volcanism
	Massimo Mattei mattei@uniroma3.it Structural analyses and volcano-tectonic expert
Opposed Reviewers:	Valerio Acocella valerio.acocella@uniroma3.it Presently in opposite project
	Giovanni Orsi Past recent research project conflicts
	Mauro Di Vito Presently involved in contrasting research project
Response to Reviewers:	According to the recommendations of the Associate Editor, we revised the manuscript as follows: -The Introduction paragraph was modified with the aim to better focalize the objectives of the paper. We highlighted the particularity of the volcanic activity of Solfatara and some of the surrounding vents, as an example of volcanism occurred in the central eastern-sector of the caldera. The main features are related to the occurrence of phreatic/phreatomagmatic explosions and the small magnitude of these events. Considering this eruption size, the Solfatara eruption becomes representative of the most likely eruptive event in case of renewal of activity at Campi Flegrei. At the same time the Solfatara area is presently the site of the most powerful hydrothermal activity at CF, so its volcanic evolution is very important for any possible future eruptive scenarios. -The stratigraphy paragraph was completely changed taking into account the comments and suggestions of the AE. In particular the stratigraphic description of the pre and post Solfatara eruptions was drastically reduced. Now this section acts as support to the legend of the geological map. On the contrary now the internal stratigraphy is more detailed, as well as tephra component characteristics, facies variation and areal distribution of Solfatara deposits. All the new data support the reconstruction of the eruptive evolution and depositional mechanisms which are part of the interpretation included in the discussion and conclusion paragraphs. The presented data contain further references on Solfatara tephra, furthermore the revised version of the Fig. 6 is more informative on the deposit dispersion. -The above mentioned changes of the two paragraphs (introduction and stratigraphy) has been performed to better focus the objective of the paper on the eruptive activity of the Solfatara volcano -Within the stratigraphy paragraph as well as in the successive paragraphs the presented data and results do not anticipate any interpretations, which are instead illustrated in the Discussion and Conclusions. -For the section dedicated to the ERT profiles we better remark the value ranges of resistivity adding these intervals in the text which in the figure are expressed in log10. We also add reference papers on the Solfatara volcano (e.g. Bruno et al., 2007; Byrdina et al., 2014) and other volcanic areas (e.g. Kagiyama et al., 1999; Lesparre et al., 2014) which report comparable values. -With the purpose of making uniform both nomenclatures and abbreviations as well as to avoid syntax errors a thorough revision of text and figures has been carried out following the specific comment and suggestions annotated on the manuscript PDF file by the Associate Editor we revise in detail the manuscript and add our modifications as follows:

main changes in the whole text:
We changed "Agnano-Monte Spina" in AMS,"MSA" in "pre-AMS", "Agnano caldera" in "AMS caldera", we eliminated the terms "maar" and "maar-diatreme" before the paragraph "6.2 Maar-diatreme structure" and we substituted those terms in "crater".

1. Introduction
we have changed the whole introduction following the suggestions of the Associated Editor.
line 40: we added these references: "(Orsi et al., 2004; Costa et al., 2009)"
lines 43-55: we changed the sentences in: "Caldera collapses of variable size occurred repeatedly through time also following not very large magma volume eruptions, as for Agnano-Monte Spina (AMS; de Vita et al., 1999). Along the SW rim of the AMS caldera (Figs. 1, 2) there is a cluster of vents within less than 2 km2, which includes Solfatara volcano. All the vents produced small magnitude explosive eruptions and lava domes. Exposed stratigraphic sequences show alternating fine to coarse ash deposits with limited distribution, scoria layers and lavas. The pyroclastic deposit characteristics suggests that these explosive vents produced both phreatic and phreatomagmatic explosions. There is no clearly observed “real” juvenile material ejected during small energetic explosions from the explosive vents of the Solfatara area (Fig. 2). Distinguishing the phreatic/hydrothermal deposits from those of the phreatomagmatic eruptions is a difficult task (Dellino et al., 2004; Pardo et al., 2009; Nemeth, 2010; Pardo et al., 2014). Determining the juvenile material is crucial to understanding the processes that define these kinds of volcanic eruptions, as well their timing and impact on the region. All this is of greater importance to characterize volcanism occurred after the high magnitude AMS eruption which in this caldera sector was reactivated through several of small magnitude events, including Solfatara. Eruptive events of this magnitude are also considered as the most likely in case of renewal of volcanism, with a probability exceeding 60% (Orsi et al., 2004; 2009). Although it is difficult to define accurately the eruptive dynamics of small-scale eruptions occurring in geothermal areas, integrating..."
line 57: we added this sentence: "Pardo et al., 2009".
lines 57-60: we moved in the end of this paragraph and changed these sentences in: " We anticipate that geological features as evolution of the eruptive phenomena, stratigraphic sequence, explosive mechanisms, crater morphology, and deformation structures at Solfatara volcano and surrounding areas are typical of maar-diatreme systems elsewhere on Earth (White, 1991; Anzidei etal., 1998; De Benedetti et al., 1998; Brand and Clarke, 2009; Pardo et al., 2009;..."
line 65: we changed the sentence "this kind of eruptions are in: "volcanoes with similar features experienced eruptions"
line 69 we changed "volcano in relation to other vents" in " volcano and its temporal and spatial relations with other vents"
line 71. we moved the sentence: " This study shows that low magnitude eruptive events led to the formation of maar-diatreme structure previously not recognized within the Campi Flegrei caldera. " in the abstract.

2. Geological background
line 81: we added: " Three main epochs of intense volcanism alternated with rest period of variable length (15.0-10.6, 9.6-9.1 and 5.5-3.8 ka, respectively) (Di Vito et al., 1999; Isaia et al., 2009; Smith et al., 2011), with the exception of the single historic eruption of Monte Nuovo (1538; Guidoboni and Ciuccarelli, 2011)."
lines 82-106: we made some minor corrections following the suggestions of the Associated Editor.
lines 106-110: we changed it in: "characterized by fine to coarse ash undulated layers and a final Strombolian activity forming a scoria cone. The Solfatara eruption was preceded also, by Monte Olibano lava dome, Paleoastroni 3 explosive eruption, Olibano Tephra phreatic eruption and Accademia lava dome (Fig. 2)."
lines 113-127: we made some minor corrections following the suggestions of the Associated Editor.

lines 129: we changed the paragraph title in:
3. Geological setting of Solfatara area
lines 130-125: we changed it in: "The geological survey, partly carried out for the new Geological Map of Naples (Foglio 447 Napoli; ISPRA 2015), allowed us to improve the knowledge on the volcano-tectonic evolution of the Solfatara area (Fig. 3)."

line 135: we changed "delineate" in " identify"

3.1 Morphology
lines 150-152: we deleted this sentence: "According to these morphological features, the Solfatara volcano can be classified as a maar (Ollier, 1967; Lorenz, 1973, Fisher and Schmincke, 1984; White and Ross, 2011)."

3.2 Stratigraphy
this paragraph has been completely rewritten in:
"The deposits outcropping along the Solfatara inner crater walls are characterized by severe hydrothermal alteration, which frequently modifies the specific lithological characteristics. Figures 3 and 4 illustrate the geological map of the analyzed area and the more representative stratigraphic logs, respectively. The N-NE sequence (Fig. 3) shows the oldest outcropping rocks, which consist of very altered pyroclastic fallout ash beds belonging to pre-AMS eruptions and the thicker and more widely exposed AMS pyroclastic density current deposits (Fig. 5d). Similar stratigraphic geometry is also visible in the very active (fumarolic) Pisciarelli area on the eastern outer flank of the Solfatara volcano (Fig. 3). The AMS and underlying deposits form an antiform structure with NW and SE dipping limbs (Figs. 3, 5d) covering a lava dome (Fig. 5 d, e) now highly altered by the fumarolic activity (Fig. 5f). A few meters above the dome, a volcanic conduit is hosted in the AMS deposits (Fig. 5d). This structure is filled by a particular type of breccia (Fig. 5a, c) including pluri-centimetric sized accretionary lapilli (Fig. 5b), rounded reworked fragments and large blocks of the host rock (AMS and pre-AMS sequence). The pipe breccias are sealed by the Olibano tephra and Solfatara sequences. Along the same cliff, Santa Maria delle Grazie scoria layer covers AMS deposits (Figs 2, 4). Monte Olibano lava dome (40-50 m thick) is covered by a coarse thick breccia (Olibano tephra; Fig. 2, Isaia et al., 2009) and Solfatara deposits in the southeastern sector of the crater (Fig. 3).
The Solfatara tephra sequence attains a maximum thickness of about 15-20 m along the N-NW crater wall and is generally characterized by massive to plane-parallel beds, in the lower part, and wavy to plane-parallel beds in the upper part. Within proximal area the centimetre thick basal coarse cohesive ash layer contains many imprints of leaves. The green to yellowish fine to coarse ash beds contain, in the lower part, abundant lapilli-size green tuff, reddish altered lava blocks and small rounded pumices, altered scoria fragments and pieces of fine ash tuff. Many clasts are coated by ash with the larger increasing in size from the base to the top up to 15 cm in diameter. Some layers have a rusty colour and contain accretionary lapilli. Among the diverse components no clear juvenile fragments was identified, as also highlighted by SEM-EDS clast analyses of a Solfatara-Averno tephra sequence at about 2 km westward from the Solfatara volcano (Fourmentraux et al., 2013). In several outcrops the Solfatara sequence contains whitish tephra layers erupted from the Averno volcano (Isaia et al., 2009). These layers are embedded at different heights along the sequence. The upper part of the Solfatara deposits is mainly composed of coarse beds or lenses and minor grey to yellowish fine-to-coarse ash beds. Juvenile material includes grey pumice fragments with feldspar, biotite and pyroxene crystals. Lithic clasts, made up by fresh and altered lavas, often rounded, and minor green and yellow tuffs and black-violet rounded scoria, reach up to 75% of the total rock volume in the breccia-like layers (Cipriani et al., 2008). Large ballistic lithic blocks (up to 1 m) are embedded in the upper part of the sequence in an area of several hundred meters around the volcano (Fig. 6b). Larger spheroidal clasts (up to several meters in diameter) display hypogene exfoliation.
The Solfatara deposits show cross laminated and undulated beds in a limited areal dispersal, up to 3 km from the vent in the westward sector (Fig. 6a). These layers, mainly correlated to the proximal upper part of the sequence, were laid down by pyroclastic density currents. The lower part of the sequence is represented by massive to plane-parallel ash beds at short distance from the vent. The preexisting topographic height in the northeastern sector of the Solfatara volcano likely favored a rapid decrease in thickness of the whole sequence. An ash fallout deposit associated to Solfatara eruption was dispersed toward N-NE at more than 7 km from the vent (Fig. 6a), consisting of alternating fine-to-coarse ash beds with intercalated, in the mid-upper part, a thin coarser lapilli pumice bed. This distal deposit mainly corresponds to the upper part of the sequence, likely containing few cm of Averno fine ash in the northern outcrops.
Both proximal and distal Solfatara deposits are covered by Astroni pyroclasts. Very fine

ash beds, forming a varve-like sequence, outcrop on the crater floor (active Fangaia mud pool; Fig. 3) and at different elevations along the southeastern margin of the Solfatara volcano. These young sediments are rich in organic remnants (e.g. carbonized wood; Fig. 6c), and testify to deposition in small pools of the strongly altered and reworked pyroclasts."

3.3 structures
line 224: we changed "are covered" in "are sealed"
line 238: we changed the sentence in: "In the NE corner of the Solfatara volcano, as described before, a lava dome crops out covered by bent pre-AMS and AMS deposits"
line 242: we changed "ductile" in "plastic"
lines 243-246: We changed the sentences in: "The overlying volcanic pipe, likely connected with the cryptodome, is characterized by sharp contacts between the AMS deposits and the pipe breccias, generally oriented in NE-SW and NW-SE directions (Fig. 5c). In the map the volcanic conduit shows a polygonal shape with a diameter of ca. 5.5 m."

4.2 Faults
line 286: we changed "as whole" in "as a whole"

4.3 Scan line data
lines 293-296: we rewritten these sentences in: "In order to provide a statistical dataset of fracture and fault attributes, such as attitudes and spacing, four scan lines were carried out. The scan line method (e.g. Guerriero et al., 2010) consists on collecting measures along a line drawn across the outcrop to be analyzed."

5. Electrical Resistivity Tomography survey
lines 323-325: we changed the sentences in: "....well outlined by electrical and electromagnetic (EM) methods. This work carried out a new ERT..."
lines 329-332: the scale in the figure is expressed in log10 than the values range between (0.2-1000 Ωm) for the profile A-A' and (1.3-158.5 Ωm) for the profile B-B'. In order to better mark these values we added these intervals in the text. These values are comparable to those reported in others papers on the Solfatara volcano (e.g. Bruno et al., 2007; Byrdina et al., 2014) or in other areas (e.g. Kagiyama et al., 1999; Lesparre et al., 2014).

6. Discussion
lines 341-342: we eliminated " the vents in the surrounding area"
lines 358-362: we changed the sentences in: " The study area hosts cross-cutting sets of regional faults with a prevalence of NW-SE and NE-SW directions (Fig. 3). Some segments of these major faults may have been reactivated during the collapse of the Solfatara crater center. For example, the SE-dipping normal fault passing for Pisciarelli (Fig. 7c), sealed by Solfatara deposits (Fig. 7b) and bounding the SE-side of Mt. Olibano, was reactivated with a reverse kinematics (Fig. 12d)."
line 375: we changed the sentence in: "with maximum activity during the various ground deformations of the CF caldera center (Di Vito et al., 1999; Isaia et al., 2009) or during the several volcanic eruptions"
line 382: we changed "As consequence" in "As a consequence"
lines 377-378: we eliminated "fractures". The sentence refers only to the faults that are almost vertical (Fig. 9r) hence well-different from the 60° of the Anderson theory.
lines 389-390: this sentence was badly written, we changed it in: " along the regional faults successively reactivated as ring faults"

6.2 Maar-diatreme structure
line 416: we added these references: (Ollier, 1967; Lorenz, 1973, Fisher and Schmincke, 1984; White and Ross, 2011)
line 420: we changed "base surges" in "pyroclastic density currents"
line 433: we added these references: "Anzidei et al., 1998; De Benedetti et al., 1998"
lines 441-443: we changed in: " The two high-resistivity (400-1000 Ωm) stairway-shaped bodies (v1) in both edges of profile A-A', both dipping to the crater center, indicate a vadose zone, unsaturated of fluids. According to these high values of resistivity, typical of magmatic intrusions (e.g. Kagiyama et al., 1999; Lesparre et al., 2014) and the Bouguer anomaly map (Bruno et al., 2007) these masses can be correlated"

6.3 Volcanic hazard implication
lines 512-532: we made minor corrections according to the suggestions of the Associate Editor.
line 535: we deleted this sentence: " These eruptions are particularly difficult to recognize in the field, and therefore to predict both in time and size. Despite"

7. Concluding remarks
we made some minor corrections in this paragraph.
we added these new references in the reference list:

Anzidei, M., Carapezza, M.L., Esposito, A., Giordano, G., Tarchini, L., and Lelli, M., 2008, The Albano Maar Lake High resolution bathymetry and dissolved CO2 budget (Colli Albani District, Italy): constrains to hazard evaluation, Journal of Volcanology and Geothermal Research, v. 171, 258-268.
Bevilacqua, A., Isaia, R., Neri, A., Vitale, S., Aspinall, W.P., Bisson, M., Flandoli, F., Baxter, P.J, Bertagnini, A., Esposti Ongaro, T., Iannuzzi, E., Pistolesi M. and Rosi, M., 2015, Quantifying volcanic hazard at Campi Flegrei caldera (Italy) with uncertainty assessment: I. Vent opening maps. Journal of Geophysical Research - Solid Earth, in press.
Cipriani, F., Marianelli, P., and Sbrana, A., 2008, Studio di una sequenza piroclastica del vulcano della Solfatara (Campi Flegrei): Considerazioni vulcanologiche e sul sistema di alimentazione: Atti Società Toscana di Scienze naturali, Memorie, Serie A, v. 113, p. 39–48.
De Benedetti, A.A., Funiciello, R., Giordano, G., Diano, G., and Caprilli, E., 2008, Volcanology history and legends of the Albano maar: In Cashman K. and G. Giordano (eds), Volcanoes and Human History, Journal of Volcanology and Geothermal Research, Spec. Vol., 176: 387-406. doi: 10.1016/j.jvolgeores.2008.04.
Fourmentraux, C., Isaia, R., Rosi, M., Sbrana, A., Bertagnini A., and Marianelli, P., 2013, Contemporaneous eruptions at 4.0 ka from 5.4 km apart vents within Campi Flegrei caldera (Southern Italy): a comparison to Rabaul caldera: 3P1_3C-O18, IAVCEI 2013 Scientific Assembly - July 20 - 24, Kagoshima, Japan
Kagiyama, T., Utada, H., and Yamamoto, T., 1999, Magma ascent beneath Unzen Volcano, SW Japan, deduced from the electrical resistivity structure: Journal of Volcanology and Geothermal Research, v. 89, p. 35-42, doi:10.1016/S0377-0273(98)00120-6.
Lesparre, N., Grychtol, B., Gibert, D., Komorowski, J. C., and Adler, A., 2014, Cross-section electrical resistance tomography of La Soufrière of Guadeloupe lava dome: Geophysical Journal International, v. 197, p. 1516-1526, doi: 10.1093/gji/ggu104.
Neri, A., Bevilacqua, A., Esposti Ongaro, T., Isaia, R., Aspinall ,W.P., Bisson, M., Flandoli, F., Baxter, P.J., Bertagnini, A. Iannuzzi, E., Orsucci, S., Pistolesi, M., Rosi, M., and Vitale, S., 2015, Quantifying volcanic hazard at Campi Flegrei caldera (Italy) with uncertainty assessment: II. Pyroclastic density current invasion maps, Journal of Geophysical Research - Solid Earth, in press.
Pardo, N., Macias, J.L., Giordano, G., Cianfarra, P., Bellatreccia, F., and Avellán, D.R., 2009. The ~1245 yr BP Asososca maar eruption: the youngest event along the Nejapa-Miraflores volcanic fault, western Managua, Nicaragua: Journal of Volcanology and Geothermal Research, v. 184, p. 292-312
Piochi, M., Kilburn, C., Di Vito, M.A., Mormone, A., Tramelli, A., Troise, C., and De Natale, G., 2014, The volcanic and geothermally active campi flegrei caldera: an integrated multidisciplinary image of its buried structure: International Journal of Earth Sciences, v. 103, p. 401-421, doi:10.1007/s00531-013-0972-7.

Figures

Figure2: we corrected "plane" in "plain", "terrrace" in "terrace" and names.
Figure6: we added the deposit thickness values for the whole measurement sites.
other figures: we made some minor corrections.

Cover Letter
Click here to download Cover Letter: Cover Letter.docx

Stratigraphy, structure and volcano-tectonic evolution of Solfatara maar-diatreme (Campi Flegrei, Italy)

Roberto Isaia[1], Stefano Vitale[2], Maria Giulia Di Giuseppe[1], Enrico Iannuzzi[1], Francesco D'Assisi Tramparulo[2], Antonio Troiano[1]

[1]Istituto Nazionale di Geofisica e Vulcanologia, sezione di Napoli Osservatorio Vesuviano, Via Diocleziano 328, 80124 Napoli, Italy

[2]Dipartimento di Scienze della Terra, dell'Ambiente e delle Risorse (DiSTAR), Università di Napoli Federico II, Largo San Marcellino 10, 80138, Napoli.

Corresponding author:

Roberto Isaia: roberto.isaia@ingv.it

Key words: maar-diatreme, phreatic eruptions, faults, volcano-tectonics, Electrical resistivity tomography, hydrothermal activity

Abstract

This study focuses on the Solfatara volcano within the Campi Flegrei, a volcanic field located in the Tyrrhenian coast of the southern Italy. Volcanism at Campi Flegrei caldera has included phreatic to phreatomagmatic explosions, and both magmatic (ranging from small scoria producing events to those with Plinian columns) and effusive eruptions. These eruptions have formed tuff cones, tuff rings, minor scoria cones and lava domes. A detailed stratigraphic, structural and geophysical study of the area indicates that the Solfatara volcano is a maar-diatreme structure previously not recognized within the Campi Flegrei caldera. It is characterized by a crater cut into earlier volcanic deposits, a small rim of ejecta and a deep structure (down to 2-3 km). This maar-diatreme has allowed to the gases and fluids to flow up to the surface over a long time. A new geological map and cross sections show a complex architecture of different volcano-tectonic features including scoria cones, lavas and cryptodomes, feeder dykes, pipes, ring and regional faults, and explosive craters. Volcanological data were collected with the main aim to characterize the eruptive activity in a limited sector of the caldera. Fault and fracture analyses, using the scan line methodology, highlight the role of the main structures that accompanied the volcanic evolution within this sector of the Campi Flegrei caldera. To better constrain the subsurface structure of the Solfatara crater, Electrical Resistivity Tomography investigations were integrated with the volcano-tectonic information. All data suggest that the Solfatara area is dominated by a maar-diatreme evolution. Presently, the Solfatara area shows a widespread hydrothermal and fumarolic activity that is localized along the major faults. The results allow us to define a particular type of volcanic activity in the recent past in the area that is still considered today as one of the areas with a higher probability of opening new vents, particularly for possible phreatic activity.

1. Introduction

Volcanic activity at Campi Flegrei (CF) has been mainly explosive. Eruptions are typically classified as phreatomagmatic and minor magmatic at variable energy scale (Orsi et al., 2004; Costa et al., 2009), forming diverse volcanic edifices (Fig. 1; e.g. Smith et al., 2011 and reference therein). Tuff cones are usually associated with a single eruptive event and tuff rings result from more complex volcano-tectonic dynamics (Isaia et al., 2004; Di Vito et al., 2011). Caldera collapses of variable size occurred repeatedly through time also following not very large magma volume eruptions, as for Agnano-Monte Spina (AMS; de Vita et al., 1999). Along the SW rim of the AMS caldera (Figs. 1, 2) there is a cluster of vents within less than 2 km^2, which includes Solfatara volcano. All the vents produced small magnitude explosive eruptions and lava domes. Exposed stratigraphic sequences show alternating fine to coarse ash deposits with limited distribution, scoria layers and lavas. The pyroclastic deposit characteristics suggests that these explosive vents produced both phreatic and phreatomagmatic explosions. There is no clearly observed “real” juvenile material ejected during small energetic explosions from the explosive vents of the Solfatara area. Distinguishing the phreatic/hydrothermal deposits from those of the phreatomagmatic eruptions is a difficult task (Dellino et al., 2004; Pardo et al., 2009; Nemeth, 2010; Pardo et al., 2014). Determining the juvenile material is crucial to understanding the processes that define these kinds of volcanic eruptions, as well their timing and impact on the region. All this is of greater importance to characterize volcanism occurred after the high magnitude AMS eruption which in this caldera sector was reactivated through several of small magnitude events, including Solfatara. Eruptive events of this magnitude are also considered as the most likely in case of renewal of volcanism, with a probability exceeding 60% (Orsi et al., 2004; 2009). Although it is difficult to define accurately the eruptive dynamics of small-scale eruptions occurring in geothermal areas, integrating knowledge on the deposits, the substrate below the volcano, and the volcano-tectonic evolution of the area, it can be possible correlate the structure of the volcano to the type of eruptions (Pardo et al., 2009; Valentine and White 2012; Kereszturi et al., 2014). The hydrothermal system beneath Solfatara volcano was active prior to its eruptive activity (Isaia et al., 2009) and is now extensively monitored (e.g. Chiodini et al., 2012) to try and understand the pre-eruptive processes in geothermal areas and their hazard. Interest in Solfatara is compounded by the fact that volcanoes with similar features experienced eruptions preceded by very short time precursors (e.g. Jolly et al., 2014) or even unregistered.

The main aim of this work is to characterize the eruptive activity and the structure of the Solfatara volcano and its temporal and spatial relations with other vents in this active sector of the Campi Flegrei caldera. We performed a multidisciplinary investigation involving a volcanological survey, deposit facies reconstruction, structural and geophysical analyses. We anticipate that geological features as evolution of the eruptive phenomena, stratigraphic sequence, explosive mechanisms, crater morphology, and deformation structures at Solfatara volcano and surrounding areas are typical of maar-diatreme systems elsewhere on Earth (White, 1991; Anzidei etal., 1998; De Benedetti et al., 1998; Brand and Clarke, 2009; Pardo et al., 2009; Sottili et al., 2012; Valentine et al., 2011; Ross et al., 2011; White and Ross, 2011; Geshi et al., 2011; Lefebvre et al., 2013; Grattinger et al., 2014; Lube et al., 2014), including those that have been recently active (e.g. Self et al., 1980; Scott and Potter, 2014). Revealing this volcanic structure takes on greater importance for an active area of the caldera that is presently experiencing active hydrothermal activity. It is also considered a vent with a higher probability of opening new vents in the future (e.g. Bevilacqua et al., 2015; Neri et al., 2015).

2. Geological background

Campi Flegrei caldera has experienced ~70 eruptions in the last 15 ka, within the collapsed area following the two major eruptive events at ~40 and ~15 ka, Campanian Ignimbrite (CI) and Neapolitan Yellow Tuff (NYT), respectively (e.g. Orsi et al., 2004; Vitale and Isaia, 2014 and reference therein; Fig.1). Three main epochs of intense volcanism alternated with rest period of variable length (15.0-10.6, 9.6-9.1 and 5.5-3.8 ka, respectively) (Di Vito et al., 1999; Isaia et al., 2009; Smith et al., 2011), with the exception of the single historic eruption of Monte Nuovo (1538; Guidoboni and Ciuccarelli, 2011). The most active vents, in both frequency and magnitude of the eruptions, have occurred in the central-eastern sector of the caldera (Vilardo et al., 2010). The more recent activity shows a series of 15 explosive and effusive eruptions over a period of 500-600 years following about 1-2 centuries of repose after the AMS Plinian eruption (AMS, about 4.5 ka calibrated age; Smith et al., 2011; Fig. 2). The renewal of volcanism was preceded by an uplift of a few tens of meters, triggered by mafic reservoir refilling at depths of 3 km or less (Isaia et al., 2009). Volcanism renewed in the central sector of the caldera, generating vents including the Solfatara volcano (Figs. 2, 3). The latter is characterized by a very intense fumarolic and hydrothermal activity both inside the crater and along the external flanks of the volcano (Pisciarelli and Via Antiniana area, Fig. 3), which makes this site as one of the most visited active volcanic areas in Europe. During the recent unrest in the CF caldera (e.g. 1982-1984; Barberi et al., 1984; Dvorak and Gasparini 1991), new fractures opened within the crater and the highest magnitude earthquakes were localized in correspondence of it (Orsi et al., 1999 and reference therein). The Solfatara-Pisciarelli-Via Antiniana area (Fig. 3) is now intensely monitored, with detailed geochemical and geophysical investigations (Bianco, et al., 2004; Caliro et al., 2007; Bruno et al., 2007; Cusano et al., 2008; Chiodini et al., 2012; Petrosino et al., 2012). However, a detailed study on the stratigraphic and structural setting of the Solfatara volcano is still lacking.

The study area (Figs. 1-3), located in the central sector of the CF caldera, about 2 km east-northeastward of Pozzuoli town, includes the Solfatara crater and the W-sector of the AMS caldera rim (Pisciarelli and Via Antiniana localities). The Solfatara crater is characterized by a sub-hexagonal shape, bounded by NW-SE, SW-NE and N-S trending ring faults (Fig. 3). This volcano formed during the most recent epoch (Epoch III) of volcanic activity at CF, at about 4200 cal. years BP (Isaia et al., 2009; Smith et al., 2011). The activity during Epoch III (5.5-3.8 ka) was dominated by explosive eruptive events, mainly located in the central-eastern caldera sector, and the only Plinian eruption of Agnano-Monte Spina (de Vita et al., 1999) at about 4.5 ka. This eruption generated a caldera collapse in the present Agnano plain (Fig. 2), and was followed by a general subsidence of the whole central sector of the caldera. The renewal of the volcanism, preceded by significant ground uplift within the CF caldera, was localized in the Solfatara area through the small latitic eruption of Santa Maria delle Grazie (4.4 ka; Isaia et al., 2009; Smith et al., 2011) (Fig. 2) characterized by fine to coarse ash undulated layers and a final Strombolian activity forming a scoria cone. The Solfatara eruption was preceded also, by Monte Olibano lava dome, Paleoastroni 3 explosive eruption, Olibano tephra phreatic eruption and Accademia lava dome (Fig. 2). All these eruptions occurred in an area close to the Solfatara volcano, mainly along the southwestern margin of the AMS collapsed area, and emitted small volumes of localized products. The Averno tuff-ring was active simultaneously with Solfatara volcano (Fig. 2; Mastrolorenzo, 1994; Di Vito et al., 2011), and is the location of the only eruption within the western sector of the caldera in the Epoch III (Isaia et al., 2009). After the Averno-Solfatara doubled events, volcanism moved northward with the Astroni and Fossa Lupara explosive eruptions, which were followed by the Nisida volcano that located along the southernmost side of the caldera margin (Fig. 2). This activity was followed by a period of quiescence that lasted more than 3000 years prior to the Monte Nuovo eruption (1538 AD) located in the western sector of the CF (Fig. 1) and which is the last eruptive event of the caldera. The Monte Nuovo eruption was preceded and accompanied by significant ground deformation, on the order of few tens of meters (Guidoboni and Ciuccarelli, 2011). Ground movements of meters have also occurred during the last century (e.g. Del Gaudio et al., 2010; Vilardo et al., 2010; D'Auria et al., 2011). Major and minor calderas as well several craters are bounded by segmented and steep ring faults, generally NW-SE and NE-SW oriented (Figs. 2-3; Vitale and Isaia, 2014). Usually, the meso-scale ring faults show dominant normal and secondarily reverse kinematics. Associated damage zones are frequently site of fumarolic activity.

3. Geological setting of Solfatara area

The geological survey, partly carried out for the new Geological Map of Naples (Foglio 447 Napoli; ISPRA 2015), allowed us to improve the knowledge on the volcano-tectonic evolution of the Solfatara area (Fig. 3). Although the rocks exposed within this sector of the Campi Flegrei are deeply affected by hydrothermal alteration, this further detailed study allowed us to define the stratigraphic relationships of the Solfatara volcano with other vents that were active after the AMS eruption. A detailed structural survey helped to identify the main faults within the area, and establish the relationships between the different structures during the growth and evolution of the volcano. The shallow structure of the Solfatara volcano was further revealed by means of Electrical

Resistivity Tomography (ERT). All these data were used to generate two geological cross sections that show the shallow structure of the investigated area, and reconstruct the geometry of the volcano at depth.

3.1 Morphology

The Solfatara crater (Fig. 3) is a small volcano (*sensu* White and Ross, 2011) having a diameter ranging between 610 and 710 m, an area of ca. 0.35 km^2, and a perimeter of ca. 2.15 km with an equivalent diameter of 665 m. The highest and lowest rim arcs are located in the NE and W sectors, respectively, with a height, from the Solfatara deposits down to the crater floor, ranging between 80 and 0 m (with a mean of 40 m). The height/crater diameter ratio is about 0.06, whereas the basal cone diameter ranges between 1.1 and 1.5 km. The well-stratified Solfatara deposits form a sub-horizontal to gently dipping (0-25°) primary slope. The eruption activity cut in the ground below the pre-eruptive surface, represented by a W-dipping flank of the Agnano Caldera. The crater is surrounded by an ejecta ring with a maximum thickness of about 30 m.

3.2 Stratigraphy

The deposits outcropping along the Solfatara inner crater walls are characterized by severe hydrothermal alteration, which frequently modifies the specific lithological characteristics. Figures 3 and 4 illustrate the geological map of the analyzed area and the more representative stratigraphic logs, respectively. The N-NE sequence (Fig. 3) shows the oldest outcropping rocks, which consist of very altered pyroclastic fallout ash beds belonging to pre-AMS eruptions and the thicker and more widely exposed AMS pyroclastic density current deposits (Fig. 5d). Similar stratigraphic geometry is also visible in the very active (fumarolic) Pisciarelli area on the eastern outer flank of the Solfatara volcano (Fig. 3). The AMS and underlying deposits form an antiform structure with NW and SE dipping limbs (Figs. 3, 5d) covering a lava dome (Fig. 5 d, e) now highly altered by the fumarolic activity (Fig. 5f). A few meters above the dome, a volcanic conduit is hosted in the AMS deposits (Fig. 5d). This structure is filled by a particular type of breccia (Fig. 5a, c) including pluri-centimetric sized accretionary lapilli (Fig. 5b), rounded reworked fragments and large blocks of the host rock (AMS and pre-AMS sequence). The pipe breccias are sealed by the Olibano tephra and Solfatara sequences. Along the same cliff, Santa Maria delle Grazie scoria layer covers AMS deposits (Figs 2, 4). Monte Olibano lava dome (40-50 m thick) is covered by a coarse thick breccia (Olibano tephra; Fig. 2, Isaia et al., 2009) and Solfatara deposits in the southeastern sector of the crater (Fig. 3).

The Solfatara tephra sequence attains a maximum thickness of about 15-20 m along the N-NW crater wall and is generally characterized by massive to plane-parallel beds, in the lower part, and wavy to plane-parallel beds in the upper part. Within proximal area the centimetre thick basal coarse cohesive ash layer contains many imprints of leaves. The green to yellowish fine to coarse ash beds contain, in the lower part, abundant lapilli-size green tuff, reddish altered lava blocks and small rounded pumices, altered scoria fragments and pieces of fine ash tuff. Many clasts are coated by ash with the larger increasing in size from the base to the top up to 15 cm in diameter. Some layers have a rusty colour and contain accretionary lapilli. Among the diverse components no clear juvenile fragments was identified, as also highlighted by SEM-EDS clast analyses of a Solfatara-Averno tephra sequence at about 2 km westward from the Solfatara volcano (Fourmentraux et al., 2013). In several outcrops the Solfatara sequence contains whitish tephra layers erupted from the Averno volcano (Isaia et al., 2009). These layers are embedded at different heights along the sequence. The upper part of the Solfatara deposits is mainly composed of coarse beds or lenses and minor grey to yellowish fine-to-coarse ash beds. Juvenile material includes grey pumice fragments with feldspar, biotite and pyroxene crystals. Lithic clasts, made up by fresh and altered lavas, often rounded, and minor green and yellow tuffs and black-violet rounded scoria, reach up to 75% of the total rock volume in the breccia-like layers (Cipriani et al., 2008). Large ballistic lithic blocks (up to 1 m) are embedded in the upper part of the sequence in an area of several hundred meters around the volcano (Fig. 6b). Larger spheroidal clasts (up to several meters in diameter) display hypogene exfoliation.

The Solfatara deposits show cross laminated and undulated beds in a limited areal dispersal, up to 3 km from the vent in the westward sector (Fig. 6a). These layers, mainly correlated to the proximal upper part of the sequence, were laid down by pyroclastic density currents. The lower part of the sequence is represented by massive to plane-parallel ash beds at short distance from the vent. The preexisting topographic height in the northeastern sector of the Solfatara volcano likely favored a rapid decrease in thickness of the whole sequence. An ash fallout deposit associated to Solfatara eruption was dispersed toward N-NE at more than 7 km from the vent (Fig. 6a), consisting of alternating fine-to-coarse ash beds with intercalated, in the mid-upper part, a thin coarser lapilli pumice bed. This distal deposit mainly corresponds to the upper part of the sequence, likely containing few cm of Averno fine ash in the northern outcrops.

Both proximal and distal Solfatara deposits are covered by Astroni pyroclasts. Very fine ash beds, forming a varve-like sequence, outcrop on the crater floor (active Fangaia mud pool; Fig. 3) and at different elevations along the southeastern margin of the Solfatara volcano. These young sediments are rich in organic remnants (e.g. carbonized wood; Fig. 6c), and testify to deposition in small pools of the strongly altered and reworked pyroclasts.

3.3 Structures

The analyzed volcanic rocks are characterized by a complex pattern of fractures and faults that acted in different times of the polyphasic volcanic history of Campi Flegrei. An early set of faults (Fig. 7a, b), hosted in the pre-AMS and AMS deposits, are sealed by the Solfatara rocks. In the Pisciarelli area (Fig. 3), the SW rim of the AMS caldera is bounded by some NW-SE normal ring faults generally sealed by younger deposits of Solfatara (Fig. 7a). A meter sized intensely fractured damage zone is well-developed close to these faults, where several fumaroles are localized (Fig.

7a). A similar geometric feature also occurs within the area between Solfatara and Pisciarelli, where an early regional NE-SW normal fault is covered by Solfatara deposits (Fig. 7b). This fault is the site of the well-known fumaroles and mud pools of Pisciarelli (Fig. 7c).

Like the AMS caldera, the central part of the Solfatara crater is bounded by several segmented steep collapse faults, generally with a normal kinematics (Fig. 7d, e) dipping towards the crater center. Frequently these planar structures produced a damage zone consisting of pervasive fractures parallel to the shear planes (Fig. 7d, e). Collapse breccias are present in some areas (Fig. 7f, g), which are characterized by centimeter to decimeter sized blocks, normally with rounded edges, embedded in a finer matrix both formed by remnants of host rock (AMS deposits).

In the NE corner of the Solfatara volcano, as described before, a lava dome crops out covered by bent pre-AMS and AMS deposits. The overlying Solfatara deposits show flat-lying strata (Fig. 5d). Geological evidences, such as (i) a steep fault located in the NW limb of this antiform structure, juxtaposing the massive lavas with beds of the pre-AMS rocks (Fig. 6e) and (ii) the plastic deformation of the overlying deposits (Fig. 5d, e), suggest that this bulging structure is a cryptodome that deformed the host rock during the lava intrusion. The overlying volcanic pipe, likely connected with the cryptodome, is characterized by sharp contacts between the AMS deposits and the pipe breccias, generally oriented in NE-SW and NW-SE directions (Fig. 5c). In the map the volcanic conduit shows a polygonal shape with a diameter of ~5.5 m.

4. Structural analysis

4.1 Fractures

Fractures generally form in two roughly orthogonal sets (F1 and F2 in the Fig. 8b, c). In places, where moderately dipping strata occur, they form a further set characterized by moderate dip angles (F3 in the Fig. 8c) frequently reactivated as normal faults (Fig. 8a). It is not rare to find highly fractured zones, not related to major faults, where the fumarole activity is focused (Fig. 8c). Normally fracture apertures are less than some millimeters in size. In the youngest deposits, fractures are aligned along the fumarole centers, such as those along the southeastern edge of Solfatara crater (Fig. 8d) that are oriented in a NE-SW direction.

About 4100 measures of planar attitudes were recorded in 74 sites (Fig. 3). Fractures, when analyzed as a whole (Fig. 9a, b), show a main N30-N210 and a secondary N110-N290 direction and the most of dip angles range between 70° and 90° (Fig. 9q). When grouped according to their spatial distribution (Fig. 9c-f), the N30-N210 direction prevails in the Solfatara crater, whereas the N110-N290 direction is dominant in the Pisciarelli area.

Finally, fractures were grouped according to the age of the hosting deposits (Fig. 9g-n). They show moderate variability in the fracture azimuths however, there are always two that are about orthogonal to the main directions.

In order to provide information about extension associated to tensile fractures, Bingham analysis (Bingham, 1974) was performed on the fracture data set. S3 eigenvectors (indicating the extension axes) are reported in the map of the analyzed area (Fig. 10a) where the contour plot of all calculated S3 vectors is also provided (Fig. 10c), suggesting a weakly prevalence of the N-S extension.

4.2 Faults

As described before, some early faults, hosted in the pre-Solfatara deposits, are sealed by the Solfatara rocks, some faults are covered by Astroni or younger deposits, and finally youngest faults cut recent sediments (Fig. 8h). Several meso-scale faults are located along the margin of the Solfatara crater and AMS caldera (Pisciarelli area). These structures show dip-separations of a few centimeters (Fig. 8e), with a maximum frequency between 5 and 50 cm (Fig. 9s), and only rarely show metric displacements. Generally all analyzed faults do not show slickenside structures; only in rare cases striations occur indicating always dip-slip kinematics (Fig. 6e, f in Vitale and Isaia, 2014). Elsewhere, faults appear as conjugate sets showing a sub-horizontal intersection (Fig. 5c). More frequently, faults are almost vertical with a maximum dip angle frequency of 80° (Fig. 9r), generally displaying normal (Figs. 7a, b, d; 8a, e-h) and occasionally reverse kinematics. Meso-scale normal faults in Astroni deposits are frequently characterized by lengths of tens of centimeters and displacements of a few centimeters (Fig. 8g). However in some localities, such as the Via Antiniana area (Fig. 3), normal faults also deform the Astroni deposits and have up to metric dip separations (Fig. 7, in Vitale and Isaia, 2014). The faults in recent sediments, such as those formed in the lacustrine deposits, show small separations (Fig. 8h) often associated with plastic deformation. When analyzed as a whole (Fig. 9o, p), the fault planes are mainly oriented in a NW-SE direction with others oriented about NNE-SSW and E-W directions, and all have high dip angles.

Extension directions from the P-B-T method (Angelier and Mechler, 1977) applied to data collected for the meso-scale normal faults, are reported in the Fig. 10a whereas the Fig. 10b shows the contour plot of T-axis, providing a main NNE-SSW direction of the extension.

4.3 Scan line data

In order to provide a statistical dataset of fracture and fault attributes, such as attitudes and spacing, four scan lines were carried out. The scan line method (e.g. Guerriero et al., 2010) consists on collecting measures along a line drawn across the outcrop to be analyzed. The first (SL1, 113 m long) was drawn about orthogonal to the E rim of the Solfatara crater (Fig. 3) where 1250 attitudes of fractures were recorded (Fig. 11a, e-j), indicating a main N15-N195 direction (Fig. 11e-h) both for the AMS (0-70 meters) and Solfatara (70-105) rocks, and a main N55-N235 and a secondary N125-N305 fracture direction (Fig. 11i-j) for the Astroni deposits (105-113 meters). The calculated fracture density (Fig. 11a) reaches a maximum close to meso-scale faults, with a background fracture density around 10-20 fractures per meters (fr/m), and maximum values of ca. 50-100 up to more than 400 fr/m in the fault-related damage zones. Rose diagrams, calculated every 10 meters, indicate a moderate variability of the main fracture direction. The second scan line (SL2) was carried out orthogonally to the SL1 (Fig. 3) in a sector lacking of major meso-scale faults (Fig. 11b, k-l). Here the fracture density is relatively low (5-40 fr/m) and fractures indicate a dominant N40-N220 direction. The third scan line (SL3) was located in a damage zone related to a ring fault in the northeastern margin of the Solfatara crater (Fig. 3). In this case, the fracture density is high everywhere (100-200 fr/m; Fig. 11c) with the main fracture direction parallel to the crater rim (N120-N300; Fig. 11m, n). The forth scan line (SL4) was drawn across the ring fault bounding the AMS caldera in the Pisciarelli area (Figs. 3, 7a). Here the fracture density increases in the fault-related damage zone, from 50-70 up to 120 fractures per meters (Fig. 11d), and subsequently decreases to 50-70 fr/m in the Solfatara deposits sealing the normal fault. These two deposits record different fracture directions, an about E-W direction prevails in the pre AMS deposits, whereas a N35-N215 direction is dominant in the Solfatara rocks. However, when analyzed together the main direction is about N100-N280 (Fig. 11o, p).

5. Electrical Resistivity Tomography survey

The Solfatara volcano has recently been surveyed by ERT (Bruno et al., 2007; Byrdina et al., 2014) and natural (MT) and controlled source (CSAMT) magnetotellurics (Bruno et al., 2007; Troiano et al., 2014). While the large-scale structure of the volcano, from a few hundred meters to a few kilometers depth, has been well imaged across MT-CSAMT profiles, the shallowest portion of the crater, from near surface to some ten meters depth, has not been well outlined by electrical and electromagnetic (EM) methods. This work carried out a new ERT survey, extending two orthogonal profiles (A-A’ and B-B’; Fig. 3) out from the crater and including the maar rim. The profiles were 550 m (A-A’) and 720 m (B-B’) long (Fig. 3). They cross the Solfatara crater following approximately the NS and EW direction, and were both carried out using 10 m electrode spacing with a maximum penetration depth of about 100 m. The resulting 2D resistivity sections are shown in Fig. 12a, c. The N-S ERT profile (A-A’, Fig. 12a) shows a moderate resistivity environment (0.2-1000 Ωm) with resistivity anomalies (v1) at the two borders. In the middle-lower area, there are alternating conductive (a1, a2 and a3) and resistive (g1, v2 and g2) layers from 0 to 100 m a.s.l. The larger conductive body (a2) is located in the proximity of the mud pool (Fangaia) at about 40 m a.s.l.. The E-W ERT profile (B-B’, Fig. 12c) also shows a moderate resistivity environment (1.3-158.5 Ωm), two large conductive bodies (a2, a3) under the mud pool, a resistive anomaly in the eastern part (v1), a resistive mass (g1) in the central-lower part and small shallower bodies close to the main fumaroles. See Appendix for further information about ERT method.

6. Discussion

The detailed volcanological and structural investigations combined with geophysical surveys of the area allowed us to further constrain the volcanic structure characterizing the Solfatara crater and fumarolic field of Pisciarelli.

6.1 Volcano-tectonic structures

The structural survey indicates that there is a temporal-spatial distribution of fractures and faults. Several structures are hosted only in the pre-Solfatara deposits; whereas others also deform Solfatara and younger rocks. Faults, outcropping in the analyzed area, can be related to the (i) volcanic explosions and collapse of the crater center (ring faults), (ii) regional tectonics and (iii) gravity instability of the volcanic rims. Ring faults (Figs. 7a, d, e; 8e) are generally from steep to sub-vertical, with predominantly normal and occasionally reverse kinematics, and are concentric showing horizontal limited extensions (less than 300 m) and tens of meters of displacement. Whereas, the regional faults (Figs. 7b, c; 8d) are several hundreds of meters long and have displacements up to a hundred meters. Faults related to gravity instabilities (Fig. 8a, g, h) are generally from a few meters to decimeters in length, with moderate to gentle dip angles and displacements less than one meter. Other minor faults with small displacements and extensions are secondary structures, related to the aforementioned fault types (Fig.7b, f) or to local extensions, such as those related to volcanic pipe development (Fig. 5c).

The study area hosts cross-cutting sets of regional faults with a prevalence of NW-SE and NE-SW directions (Fig. 3). Some segments of these major faults may have been reactivated during the collapse of the Solfatara crater center. For example, the SE-dipping normal fault passing for Pisciarelli (Fig. 7c), sealed by Solfatara deposits (Fig. 7b) and bounding the SE-side of Mt. Olibano, was reactivated with a reverse kinematics (Fig. 12d). According to the CO_2 flux maps (e.g. Todesco et al., 2003; Byridina et al., 2014), most of fumaroles are focused along these faults, such as those running along the NE and SE rim of Solfatara crater (Fig. 10a), or in the intersection between major faults (e.g., the main fumaroles of Bocca Grande and Pisciarelli; Fig. 10a). The estimation of density fractures across these ring faults by means of the scan line method (Fig. 11) revealed highly fractured damage zones, several meters in size, characterized by more than 100 fractures per meter. These structures are located along both the crater rim and in the collapsed central sector, as suggested by the ERT profiles, forming highly permeable corridors and preferred pathways for fluids and gases. Similar to the faults, the fractures show similar main NE-SW and NW-SE directions for all deposits, and secondarily WNW-ESE and NNE-SSE directions. These dominant trends are also consistent with the main directions of mapped faults (Fig. 3). According to Vitale and Isaia (2014), the process of tensile fracturing was continuous during the whole evolution of Campi Flegrei, with maximum activity during the various ground deformation episodes of the CF caldera center (Di Vito et al., 1999; Isaia et al., 2009) or during the several volcanic eruptions. Faults are mostly vertical (Fig. 9q), being characterized by a mean dip of 80° (Fig. 9r). The latter value differs from the theoretical value of 60° (Anderson, 1905) for the neo-formed normal shear planes close to the Earth surface. High angle faults are very common in the volcanic settings and sometimes show reverse kinematics (e.g. Acocella, 2007; Vitale and Isaia, 2014). Normal fault enucleated in the basement can get steeper toward the surface (e.g. Holland et al., 2011) or join up with steep pre-existing fractures, producing very high-angle faults (e.g. Hardy, 2013). As a consequence, the development of the Solfatara crater, with the consequent collapse of the inner zone, was hardly influenced by the inherited structures. The collapse reactivated the pre-existing fractures along the well-known regional NW-SE and NE-SW and secondarily WNW-ESE and NNE-SSE directions (e.g. Vitale and Isaia, 2014). This strong influence of inherited structures, characterized by preferred planar directions, has also had an impact on the crater morphology that is hexagonal in shape (Fig. 3).

It is worth noting that the area comprising Solfatara crater, Pisciarelli and Via Antiniana (Fig. 3) has fumaroles and gas emissions that are mainly localized along the regional faults successively reactivated as ring faults (Fig. 10a). In particular, the main centers are located along the intersections of largest structures. For example, the Pisciarelli fumaroles and mud pool are located in the crossing between the regional NE-SW and NW-SE faults, the latter reactivated as ring faults during the AMS caldera collapse (Isaia et al., 2009), or in Via Antiniana (Fig. 10a) where fumaroles are localized in the intersections between the NE-SW, NW-SE and WNW-ESE faults (Fig. 10a).

Fractures normally appear as two orthogonal sets, with one more developed, as a consequence of (i) a local switch between the intermediate (σ2) and the minimum (σ3) stress axes close to the growing fractures (Guerriero et al., 2011), or (ii) a tensile regime including two orthogonal extensions localized in the uppermost crust as consequence of the resurgence of the central sector of CF caldera during the last 4500 years BP (e.g. Del Gaudio et al., 2010) and/or to local uplift and collapse related to the volcanic explosions. These fracture sets are also present in the recent deposits located in the Solfatara crater, indicating similar preferred orientations (Fig. 9m, n), probably associated to the latest bradeisismic activity (e.g. Acocella et al., 1999). The extension directions (T and S3 axes) estimated by P-B-T (faults) and Bingham (fractures) analysis suggest an almost radial pattern, with prevalence of a NNE-SSW extension for the T-axis and a N-S extension for the S3-axis (Fig. 10b, c). On the map (Fig. 10a), the T and S3 axes often show different directions at the same site (at some locations there is also 90° of difference). This angular discrepancy is probably related to the occurrence of two orthogonal sets of fractures as well as to the radial pattern of the collapse extension and volcanic explosion fragmentation.

6.2 Maar-diatreme structure

Several morphological, volcanic, sedimentary and structural features indicate that the shallow structure of the Solfatara crater is a maar (Ollier, 1967; Lorenz, 1973, Fisher and Schmincke, 1984; White and Ross, 2011); these include:

- the small size of the crater (with a mean diameter of 665 m), with the floor lying below the pre-eruptive surface (i.e. the AMS and Accademia deposits) and surrounded by an ejecta ring deposited on the pre-eruptive ground around the crater;
- Solfatara deposits are largely represented by phreatic and phreato-magmatic ash, lapilli and breccias, and lava flows are lacking;
- there is a high proportion of non-juvenile fragments in the basal part of the sequence;
- the pyroclasts have been emplaced by pyroclastic density currents and minor fallout and accretionary lapilli are very common;
- the contacts with the pre-existing rocks are generally abrupt and defined by collapse (ring) faults with damage zones that have high fracture densities (normally 100-200 fractures/m);
- scoria cone, lava domes and a cryptodome are found in the crater, but predate the Solfatara eruption.
- collapse breccias, formed by large block and finer wall rock matrix, are locally preserved along the ring faults and in a small volcanic conduit observed at the top of the cryptodome;

Generally, a maar is connected to a deeper root zone through a diatreme (White and Ross, 2011 and reference therein). Presently information about maar-diatreme structures and volcanic evolution are provided by ancient (Hearn, 1968; White, 1991; Anzidei et al., 1998; De Benedetti et al., 1998; Brand and Clarke, 2009; Valentine et al., 2011; Ross et al., 2011; White and Ross, 2011; Lefebvre et al., 2013) and active (Kienle et al., 1980; Self et al., 1980; Geshi et al., 2011;) volcanoes or through blast experiments (Goto et al., 2001; White and Ross, 2011; Valentine, 2012; Valentine and White, 2012; Graetting et al., 2014).

Normally the diatreme shape is an inverted cone that develops with a vertical length that is 1-4 times the diameter (e.g. Tamas and Milesi, 2002; Lorenz, 2007; White and Ross, 2011), the latter generally being in order of few hundred of meters to 2-3 km in size.

We can observe the shallow diatreme structure (down to 100 m of depth) of the Solfatara volcano in the ERT, A-A' and B-B', profiles (Fig. 12a, c). The two high-resistivity (400-1000 Ωm) stairway-shaped bodies (v1) in both edges of profile A-A', both dipping to the crater center, indicate a vadose zone, unsaturated of fluids. According to these high values of resistivity, typical of magmatic intrusions (e.g. Kagiyama et al., 1999; Lesparre et al., 2014) and the Bouguer anomaly map (Bruno et al., 2007) these masses can be correlated to the two lava domes bounding the Solfatara crater (Monte Olibano to the south and the Solfatara cryptodome to the north). The stairway shape can be interpreted as steep concentric ring faults, such as shown in the geological section A''-A''' (Fig. 12b). These collapse faults show dip separations ranging between 10 and 50 m. Low-resistivity bodies (a1, a2 and a3) located in the lower, middle and upper part of ERT profile (Fig. 12a) are interpreted as aquifers, i.e. fluid saturated permeable rocks. The a2 and a3 low-resistivity bodies are hosted in the Solfatara and Astroni deposits, respectively. The moderate resistivity level (v2), located at 60-80 m depth, appears to be a partially fluid saturated layer corresponding to the upper part of the Solfatara deposits made of breccias containing low-permeable lava boulders. The two moderate resistivity masses located in the central part at 0-40 m depth are interpreted as the gas-saturated level, segmented by faults, that connects to a deeper rich-gas root zone. The superficial level (g2), characterized by a higher resistivity with respect the surrounding rocks, marks recent sediments gas saturated.

The ERT profile B-B’ (Fig. 12c) shows a highly resistive body (v1) probably westward bounded by a ring fault. This mass can be correlated to the Solfatara cryptodome cropping out in the NE corner of Solfatara crater and can be seen in the section B’’-B’’’ (Fig. 12d). The large low-resistivity area (a2) in the right side of the profile, located between 0 and 50 m can be assumed as a highly fractured body fluids saturated. It forms a hydrothermal conductive plume below the Fangaia (Byrdina et al., 2014) of upwelling fluids from a large water table located at about 0-30 m depth (Bruno et al., 2007).

Such as the previous ERT profile A-A’, the moderate resistivity masses (v2) located at 60 m (a.s.l.) are interpreted as the upper part of the Solfatara deposits, whereas levels (a3) and (g2) correspond to the Astroni and recent deposits, respectively; the first containing fluids and the latter saturated of gases. Fluids emerge from the mud pool (Fangaia). Finally the low resistivity masses (g2), located along the NE margin, correspond to water-saturated AMS deposits.

These results, added to the previous knowledge (e.g. Chiodini et al., 2003; Bruno et al., 2007; Byrdina et al., 2014), outline a complex hydrothermal system localized in the Solfatara crater including a mix of upwelling fluids, gases and meteoric water (Fig. 12b, d). The collapsed central sector of the Solfatara crater hosts interfering gas and fluid flows driven by the rock permeability. The main flow paths are localized in highly fractured rocks that are the result of explosive activity and collapse faulting.

The Fig.13a shows a model of the Solfatara diatreme down to a depth of 2-3 km. The structure includes an upper zone consisting of a maar crater with rims made of lava domes, cryptodomes and tephra deposits. The central sector is filled, from the surface to deep, by post-eruptive sediments, syn-eruptive collapse breccias, and finally by more or less dismembered rocks of substrate. The crater rim forms a stair-step-like structure cut by concentric steep segmented ring faults. According with the available diatreme models (e.g. Lorenz, 1986; White, 1991; White and Ross, 2011) and the magnetotelluric surveys across the Solfatara volcano (Troiano et al., 2014), which outline a deep structure marked by a high resistivity conduit down to 3 km where a similar horizontal panel is present (Fig. 13b), we can envisage (i) a lower zone consisting of disrupted beds and a central gas-saturated high resistivity conduit; (ii) a root zone where the conduit enlarges into a highly fractured area that joins a feeder dike, sill or magmatic chamber.

Further geological evidence supporting the diatreme model is the persistence of long-lived hydrothermal activity. Altered lithic clasts in the Solfatara deposits suggest that there was an active hydrothermal system before the explosive eruption occurred at ~4200 years BP (Isaia et al., 2009; Smith et al., 2011). Furthermore, fumarolic activity was recorded in the Roman time by the Greek geographer Strabo (63/64 BCE-24 CE; Scandone et al., 2010).

The volcano-tectonic evolution of Solfatara, like other maar-diatreme volcanoes (Hearn, 1968; Houser, 1969; Ross et al., 2011), is a combination of explosive and collapse processes. The occurrence in the Solfatara ejecta deposits of shallow large rounded and exfoliated lithics (more than 1 m in size) and deep-seated lithic fragments including the green tuff recognized below the AMS and pre-AMS sequences along the Pozzuoli coast (La Pietra tuffs; Di Vito et al., 1999) and from subsurface data within the Agnano Plain (Piochi et al., 2014), indicates multiple volcanic explosions at various depths (Graetting et al., 2014). According to Ross and White (2006) and Ross et al., (2008a, b), the material located in lower part of the volcano could be ejected through the "debris jets" phenomenon, consisting in (i) deep-seated explosions producing a gradual upward transport in the diatreme, with the fragmentation, size-reduction and mixing with other lithics located at various depths (clast recycling; Houghton and Smith, 1993; Lefebvre et al., 2013) and (ii) shallow explosions that ejected the lithics out of the crater (Graetting et al., 2014). Finally, we suggest for the Solfatara volcano a maar-diatreme evolution including: (i) early deep explosions that excavated the pre-eruption basement, (ii) later multiple shallow explosions that allowed the ejection of reworked lithics, and (iii) other shallow explosions probably located in other sector of the crater involving undeformed rocks and producing the ejection of breccias with large boulders out of the crater. It follows that the explosions migrated both vertically and laterally such as described in other maar-diatremes (e.g. Son et al., 2012). This explosive activity was assisted by the collapse of the host rock and formed the crater rims, presently attested by the wide spectrum of structures such as ring faults and related damage zones, collapse breccias, pervasive fractures, and minor faults.

6.3 Volcanic hazard implication

The new data here presented show that Solfatara volcano has experienced mainly phreatic and small phreatomagmatic events, which followed a few smaller phreatic, phreatomagmatic and lava dome-forming eruptions in the area around the present crater rim. This very intense volcanism concentrated in this sector of the CF caldera was firstly active on the southwestern edge of the AMS eruption caldera collapse. The Solfatara volcano grew at the end of a series of eruptive events, which also contributed to the formation of a maar-diatreme structure (e.g. Geshi et al., 2011). It is difficult to identify the eruption mechanisms dealing with very altered deposits, also characterized by local dispersion. The very recent eruption crises occurred at Mt. Tongariro, New Zealand, experienced a similar volcanic evolution to that of Solfatara and the analyzed deposits also show the difficulties in defining the eruption style (Pardo et al., 2014).The identification of this type of volcanism and structure shows that phreatic events and emplacement of lava domes are eruptions common within this sector of the CF caldera.

Structural and geophysical investigations show that Solfatara area is dominated by a maar-diatreme volcanic structure. The area hosts many faults and related highly fractured damage zones of different ages as well as a widespread hydrothermal and fumarolic field (e.g. Caliro et al., 2007). The main fumaroles and mud pools are concentrated inside the Solfatara crater and in the Pisciarelli site, generally aligned along the major structures and at their crossings. The Pisciarelli area has experienced significant variations in the last 10 years, consisting in a widening of the hydrothermal area and an increase in temperature and magmatic gas emission of the fumaroles (Chiodini et al., 2012). Our results highlight the occurrence of volcano-tectonic features for the Solfatara area, suggesting that phreatic eruptions and/or small phreatomagmatic events, similar to those documented from the 2012 Te Maari eruption in New Zealand (e.g. Cronin et al., 2014), pose a high volcanic risk to this densely populated area. This type of volcanism that has occurred in the Solfatara-Pisciarelli area needs to be considered among the possible eruptive scenarios in case of renewal of volcanism at CF.

7. Concluding remarks

- The Solfatara volcano grew after a quite intense volcanism from vents in close proximity. These vents generated small explosive phreatic and phreatomagmatic eruptions and lava and crypto-domes.
- The Solfatara eruptive sequence was characterized by an initial phreatic phase, followed by discrete explosions involving magmatic activity that formed pyroclastic currents, distributed around the vent area, and fallout ash deposits from low eruptive columns.
- Some volcano-tectonic features such as collapsed breccias, volcanic conduits, and cryptodome were described for the first time in the Solfatara volcano.
- Morphological, stratigraphic and structural analyses integrated with data from geo-electrical surveys suggest that the Solfatara volcano is a maar-diatreme structure. It is characterized by a shallow crater, cut in the pre-eruptive basement, and a deep diatreme (down to 2-3 km). The upper zone comprises desegregated rocks and collapse breccias, which form a stair-step-like structure that is cut by concentric steep ring faults, and the lower sector is where the gas-saturated conduit joins the root zone that is connected to a magmatic source.

- Ring faults, related to the collapse of the inner part of the maar-diatreme, are strongly influenced by inherited structures frequently resulting as reactivation of segments of preexistent regional faults characterized by the well-known Apennine (NW-SE) and Anti-Apennine (NE-SW) directions.
- The ERT survey, consisting of two almost orthogonal profiles (~N-S and ~E-W) crosscutting the maar rims, further clarifies the underground structure of the Solfatara volcano. It outlines a complex hydrothermal system, formed by a mix of upwelling fluids, gases and meteoric water. The preferred pathways, highlighted by scan-line surveys, for fluids and gases are located both along the crater rim and in the collapsed central sector where highly fractured rocks occur.
- A new geological map of the Solfatara area and relative cross sections across the area are presented.
- The stratigraphy of ejecta indicates an eruption evolution of the Solfatara maar-diatreme with the explosions migrated both vertically and laterally. The early explosions were deep and excavated the pre-eruption basement, and were followed by multiple shallow explosions that ejected recycled lithics, generating breccias with large boulders.
- The type volcanism that occurred in past at the Solfatara area should be considered as a future eruption scenario at Campi Flegrei. The Solfatara-Pisciarelli area is in sector of the caldera that has the maximum probability of opening of new vent and is presently the site of most intense fumarolic and hydrothermal manifestation.

Acknowledgments

We thank Karoly Nemeth and an anonymous reviewer as well as Editor Guido Giordano for the extremely useful comments and suggestions that significantly improved this paper. Manuscript greatly benefited of the English editing and suggestions by V. C. Smith (Oxford University, UK).

Special thanks to Carlo Scirocco, and Francesco Cappuccio for the help during field work. This work was partly funded by the Italian Department of Civil Defence Protection within framework DPC-INGV 2012-2021, Volcanological Project V1.

Reference list

Acocella, V., 2007, Understanding caldera structure and development: An overview of analogue models compared to natural calderas: Earth Science Reviews, v. 85, p.125-160, doi: 10.1016/j.earscirev.2007.08.004

Acocella, V., Salvini, F., Funiciello, R., and Faccenna, C., 1999, The role of transfer structures on volcanic activity at Campi Flegrei Southern Italy: Journal of Volcanology and Geothermal Research, v. 91, p. 123–139, doi: 10.1016/S0377-0273(99)00032-3

Angelier, J., and Mechler, P., 1977, Sur une methode graphice de recherche des contraintes principales egalement utilisable en tectonique et en seismologie: la methode des diedres droits: Bulletin Societé Geologique France XIX, v.7, p.1309-1318.

Anzidei, M., Carapezza, M.L., Esposito, A., Giordano, G., Tarchini, L., and Lelli, M., 2008, The Albano Maar Lake High resolution bathymetry and dissolved CO2 budget (Colli Albani District, Italy): constrains to hazard evaluation, Journal of Volcanology and Geothermal Research, v. 171, 258-268.

Barberi, F., Corrado, G., Innocenti, F., and Luongo, G., 1984, Phlegraean Fields 1982–1984: Brief chronicle of a volcano emergency in a densely populated area: Bullettin of Volcanology, v. 47(2), p.175–185, doi: 10.1007/BF01961547

Bevilacqua, A., Isaia, R., Neri, A., Vitale, S., Aspinall, W.P., Bisson, M., Flandoli, F., Baxter, P.J, Bertagnini, A., Esposti Ongaro, T., Iannuzzi, E., Pistolesi M. and Rosi, M., 2015, Quantifying volcanic hazard at Campi Flegrei caldera (Italy) with uncertainty assessment: I. Vent opening maps. Journal of Geophysical Research - Solid Earth, in press.

Bianco, F., Del Pezzo, E., Saccorotti, G., and Ventura, G., 2004, The role of hydrothermal fluids in triggering the July August 2000 seismic swarm at Campi Flegrei, Italy: Evidence from seismological and mesostructural data: Journal of Volcanology and Geothermal Research, v. 133, p. 229–246, doi:10.1016/S0377-0273(03)00400-1.

Bingham, C., 1974, An antipodally symmetric distribution on the sphere: Annals of Statistics, v. 2, p. 1201–1225.

Brand, B.D., and Clarke, A.B., 2009, The architecture, eruptive history, and evolution of the Table Rock Complex, Oregon: From a Surtseyan to an energetic maar eruption: Journal of Volcanology and Geothermal Research, v. 180, p. 203–224, doi:10.1016/j.jvolgeores.2008.10.011.

Bruno, P.G., Ricciardi, G.P., Petrillo, Z., Di Fiore, V., Troiano, A., and Chiodini, G., 2007, Geophysical and hydrogeological experiments from a shallow hydrothermal system at Solfatara Volcano, Campi Flegrei, Italy: Response to caldera unrest: Journal of Geophysical Research, v. 112, B06201, doi: 10.1029/2006JB004383.

Byrdina, S., Vandemeulebrouck, J., Cardellini, C., Legaz, A., Camerlynck, C., Chiodini, G., Lebourg, T., Gresse, M., Bascou, P., Motos, G., Carrier, A., and Caliro, S., 2014, Relations between electrical resistivity, carbon dioxide flux, and self-potential in the shallow hydrothermal system of Solfatara (Phlegrean Fields, Italy): Journal of Volcanology and Geothermal Research, v. 283, p. 172–182.

Caliro, S., Chiodini, G., Moretti, R., Avino, R., Granieri, D., Russo, M., and Fiebig, J., 2007, The origin of the fumaroles of La Solfatara (Campi Flegrei, south Italy): Geochimica et Cosmochimica Acta, v. 71, p. 3040–3055, doi:10.1016/j.gca.2007.04.007.

Chiodini, G., Todesco, M., Caliro, S., Del Gaudio, C., Macedonio, G., and Russo, M., 2003, Magma degassing as a trigger of bradyseismic events: The case of Phlegrean Fields (Italy), Geophys. Res. Lett., v. 30, p. 1434, doi:10.1029/2002GL016790.

Chiodini, G., Caliro, S., De Martino, P., Avino, R., and Gherardi, F., 2012. Early signals of new volcanic unrest at Campi Flegrei caldera? Insights from geochemical data and physical simulations: Geology, v. 40, p. 943-946, doi: 10.1130/G33251.1

Cipriani, F., Marianelli, P., and Sbrana, A., 2008, Studio di una sequenza piroclastica del vulcano della Solfatara (Campi Flegrei): Considerazioni vulcanologiche e sul sistema di alimentazione: Atti Società Toscana di Scienze naturali, Memorie, Serie A, v. 113, p. 39–48.

Cronin, S.J., Stewart, C., Zernack, A.V., Brenna, M., Procter, J.N., Pardo, N., Christenson, B., Wilson, T., Stewart, R.B., and Irwin, M., 2014, Volcanic ash leachate compositions and assessment of health and agricultural hazards from 2012 hydrothermal eruptions, Tongariro: New Zealand, Journal of Volcanology and Geothermal Research, v. 286, p. 233–247, doi:10.1016/j.jvolgeores.2014.07.002.

Cusano, P., Petrosino, S., and Saccorotti, G., 2008, Hydrothermal origin for sustained long-period (LP) activity at Campi Flegrei Volcanic Complex, Italy: Journal of Volcanology and Geothermal Research, v. 177, p. 1035–1044, doi:10.1016/j.jvolgeores.2008.07.019.

Dahlin, T., and Zhou, B., 2004, A numerical comparison of 2D resistivity imaging with 10 electrode arrays: Geophysical Prospection, v. 52, p. 379-398, doi: 10.1111/j.1365-2478.2004.00423.x.

D'Auria, L., Giudicepietro, F., Aquino, I., Borriello, G., Del Gaudio, C., Lo Bascio, D., Martini, M., Ricciardi, G. P., Ricciolino, P., and Ricco, C., 2011, Repeated fluid-transfer episodes as a mechanism for the recent dynamics of Campi Flegrei caldera (1989–2010): Journal of Geophysical Research, v. 116, B04313, doi:10.1029/2010JB007837.

Del Gaudio, C., Aquino, I., Ricciardi, G.P., Ricco, C., and Scandone, R., 2010, Unrest episodes at Campi Flegrei: a reconstruction of vertical ground movements during 1905–2009: Journal of Volcanology and Geothermal Research, v. 185, p. 48–56, doi: 10.1016/j.jvolgeores.2010.05.014

Dellino, P., Isaia, R., La Volpe, L., and Orsi, G., 2004, Interference of particles fallout on the emplacement of pyroclastic surge deposits of the Agnano-Monte Spina eruption (Phlegraean Fields, Southern Italy), Journal of Volcanology and Geothermal Research, v.133, p. 193-210, doi:10.1016/S0377-0273(03)00398-6.

De Benedetti, A.A., Funiciello, R., Giordano, G., Diano, G., and Caprilli, E., 2008, Volcanology history and legends of the Albano maar: In Cashman K. and G. Giordano (eds), Volcanoes and Human History, Journal of Volcanology and Geothermal Research, Spec. Vol., 176: 387-406. doi: 10.1016/j.jvolgeores.2008.04.

de Vita, S., Orsi, G., Civetta, L., Carandente, A., D'Antonio, M., Di Cesare, T., Di Vito, M., Fisher, R.V., Isaia, R., Marotta, E., Ort, M., Pappalardo, L., Piochi, M., and Southon, J., 1999, The Agnano-Monte Spina eruption (4.1 ka) in the resurgent, nested Campi Flegrei caldera (Italy): Journal of Volcanology and Geothermal Research, v. 91, p. 269–301.

Di Maio, R., Mauriello, P., Patella, D., Petrillo, Z., Piscitelli, S., Siniscalchi, A., and Veneruso, M., 1997, Self-potential, geoelectric and magnetotelluric studies in Italian active volcanic areas: Annals of Geophysics, v. 40, p. 519-537, doi: 10.4401/ag-3926.

Di Maio, R., Mauriello, P., Patella, D., Petrillo, Z., Piscitelli, S., and Siniscalchi, A., 1998, Electric and electromagnetic outline of the Mount Somma-Vesuvius structural setting: Journal of Volcanology and Geothermal Research, v. 82, p. 219-238, doi: 10.1016/S0377-0273(97)00066-8.

Di Vito, M.A., Arienzo, I., Braia, G., Civetta, L., D’Antonio, M., Di Renzo, V., and Orsi G., 2011, The Averno 2 fissure eruption: a recent small-size explosive event at the Campi Flegrei caldera (Italy): Bullettin of Volcanology, v. 73, p. 295-320, doi: 10.1007/s00445-010-0417-0.

Dvorak, J.J., and Gasparini, P., 1991, History of earthquakes and vertical ground movement in Campi Flegrei caldera, Southern Italy: comparison of precursory events to the A.D. 1538 eruption of Monte Nuovo and of activity since 1968: Journal of Volcanology and Geothermal Research, v. 48, p. 77-92.

Fikos, I., Vargemezis, G., Zlotnicki, J., Puertollano, J.R., Alanis, P.B., Pigtain, R.C., Villacorte, E.U., Maliport, G.A., and Sasai, Y., 2012, Electrical resistivity tomography study of Taal volcano hydrothermal system, Philippines: Bullettin of Volcanology, v. 74, p. 1821-1831, doi: 10.1007/s00445-012- 0638-5.

Fourmentraux, C., Isaia, R., Rosi, M., Sbrana, A., Bertagnini A., and Marianelli, P., 2013, Contemporaneous eruptions at 4.0 ka from 5.4 km apart vents within Campi Flegrei caldera (Southern Italy): a comparison to Rabaul caldera: 3P1_3C-O18, IAVCEI 2013 Scientific Assembly - July 20 - 24, Kagoshima, Japan

Geshi, N., Németh, K., and Oikawa, T., 2011, Growth of phreatomagmatic explosion craters: A model inferred from Suoana crater in Miyakejima Volcano, Japan: Journal of Volcanology and Geothermal Research, v. 201, p. 30–38, doi:10.1016/j.jvolgeores.2010.11.012.

Goto, A., Taniguchi, H., Yoshida, M., Ohba, T., and Oshima, H., 2001, Effects of explosion energy and depth to the formation of blast wave and crater: Field explosion experiment for the understanding of volcanic explosion: Geophysical Research. Letters, v. 28, p. 4287–4290.

Guerriero V., Iannace A., Mazzoli S, Parente M, Vitale S., and Giorgioni M., 2010. Quantifying uncertainties in multi-scale studies of fractured reservoir analogues: Implemented statistical analysis of scan line data. Journal of Structural Geology 32, 1271-1276, doi: 10.1016/j.jsg.2009.04.016

Guerriero, V., Vitale, S., Ciarcia, S., and Mazzoli, S., 2011, Improved statistical multi-scale analysis of fractured reservoir analogues: Tectonophysics, v. 504, p. 14-24, doi:10.1016/j.tecto.2011.01.003

Guidoboni, E., and Ciuccarelli, C., 2011, The Campi Flegrei caldera: historical revision and new data on seismic crises, bradyseisms, the Monte Nuovo eruption and ensuing earthquakes (twelfth century 1582 ad): Bullettin of Volcanology, v. 73, p. 655–677. doi:10.1007/s00445-010-0430-3

Hardy, S., 2013, Propagation of blind normal faults to the surface in basaltic sequences: Insights from 2D discrete element modelling: Marine and Petroleum Geology doi:10.1016/j.marpetgeo.2013.08.012.

Hearn, C.B., 1968, Diatremes with Kimberlitic affinities in North-Central Montana: Science, v. 159(3815), p. 622–625.

Holland, M., van Gent, H., Bazalgette, L., Yassir, N., Hoogerduijn Strating, E.H., and Urai, J.L., 2011, Evolution of dilatant fracture networks in a normal fault — Evidence from 4D model experiments: Earth and Planetary Science Letters, v. 304, p. 399–406, doi:10.1016/j.epsl.2011.02.017.

Houghton, B.F., and Smith, R.T., 1993, Recycling of magmatic clasts during explosive eruptions: Estimating the true juvenile content of phreatomagmatic volcanic deposits: Bullettin of. Volcanology, v. 55, p. 414–420.

Isaia, R., D’Antonio, M., Dell’Erba, F., Di Vito, M., and Orsi, G., 2004, The Astroni volcano: the only example of close eruptions within the same vent area in the recent history of of the Campi Flegrei caldera (Italy): Journal of Volcanology and Geothermal Research, v. 133, p. 171-192, doi:10.1016/S0377-0273(03)00397-4

Isaia, R., Marianelli, P., and Sbrana, A., 2009, Caldera unrest prior to intense volcanism in Campi Flegrei (Italy) at 4.0 ka B.P.: implications for caldera dynamics and future eruptive scenarios: Geophysical Research Letters, v. 36:L21303, doi:10.1029/2009GL040513.

ISPRA, 2015, Carta Geologica d'Italia, Foglio 447 Napoli, http://www.isprambiente.gov.it/Media/carg/447_NAPOLI/Foglio.html

Kagiyama, T., Utada, H., and Yamamoto, T., 1999, Magma ascent beneath Unzen Volcano, SW Japan, deduced from the electrical resistivity structure: Journal of Volcanology and Geothermal Research, v. 89, p. 35-42, doi:10.1016/S0377-0273(98)00120-6.

Kereszturi, G., Németh, K., Cronin, S.J., Procter, J., and Agustín-Flores, J., 2014, Influences on the variability of eruption sequences and style transitions in the Auckland Volcanic Field, New

Zealand: Journal of Volcanology and Geothermal Research, v. 286, p. 101-115, doi:10.1016/j.jvolgeores.2014.09.002.

Kienle, J., Kyle, P.R., Self, S., Motyka, R.J., and Lorenz, V., 1980, Ukinrek Maars, Alaska, I. April 1977 eruption sequence, petrology and tectonic setting: J. Volcanol. Geotherm. Res., v. 7, p. 11–37.

Jolly, A.D., Jousset, P., Lyons, J.J., Carniel, R., Fournier, N., Fry, B., and Miller, C., 2014. Seismoacoustic evidence for an avalanche driven phreatic eruption through a beheaded hydrothermal system: an example from the 2012 Tongariro eruption: Journal of Volcanology and Geothermal Research, v. 286, p. 331–347, doi:10.1016/j.jvolgeores.2014.04.007.

Lefebvre, N.S., White, J.D.L., and Kjarsgaard, B.A., 2013, Unbedded diatreme deposits reveal maar-diatreme forming eruptive processes: Standing Rocks West, Hopi Buttes, Navajo Nation, USA: Bullettin of Volcanology, v. 75(8), p. 739, doi:10.1007/s00445-013-0739-9.

Lesparre, N., Grychtol, B., Gibert, D., Komorowski, J. C., and Adler, A., 2014, Cross-section electrical resistance tomography of La Soufrière of Guadeloupe lava dome: Geophysical Journal International, v. 197, p. 1516-1526, doi: 10.1093/gji/ggu104.

Legaz, A.V., Vandemeulebrouck, J.R., Revil, A., Kemna, A., Hurst, A.W., Reeves, R., and Papasin, R., 2009, A case study of resistivity and self-potential signatures of hydrothermal instabilities, Inferno Crater Lake, Waimangu: New Zealand Geophysical Research Letters, v. 36, L12306, doi: 10.1029/ 2009GL037573.

Li, Y., and Oldenburg, D.W., 1992, Approximate inverse mappings in DC resistivity problems: Geophysical Journal International, v. 109, 343-362, doi: 10.1111/j.1365-246X.1992.tb00101.x.

Loke, M.H., 2012, Tutorial: 2-D and 3-D electrical imaging surveys: Geotomo Softwares, Penang, Malaysia, 1-161.

Loke, M.H., and Barker, R.D., 1995, Least-squares deconvolution of apparent resistivity pseudosections: Geophysics, v. 60, p. 1682–1690, doi: 10.1190/1.1443900.

Loke, M.H., and Barker, R.D., 1996, Rapid least-squares inversion of apparent resistivity pseudosections by a quasi-Newton method: Geophysical Prospection, v. 44, p. 131-152, doi: 10.1111/j.1365- 2478.1996.tb00142.x.

Lorenz, V., 1986, On the growth of maars and diatremes and its relevance to the formation of tuff rings: Bulletin of Volcanology, v. 48, p. 265–274.

Lorenz, V., 2007, Syn- and posteruptive hazards of maar–diatreme volcanoes: Journal of Volcanology and Geothermal Research, v. 159, p. 285–312, doi: 10.1016/j.jvolgeores.2006.02.015.

Lube, G., Breard, E.C.P., Cronin, S.J., Procter, J.N., Brenna, M., Moebis, A., Pardo, N., Stewart, R.B., Jolly, A., and Fournier, N., 2014, Dynamics of surges generated by hydrothermal blasts during the 6 August 2012 Te Maari eruption, Mt Tongariro, New Zealand: Journal of Volcanology and Geothermal Research, v. 286, p. 348–366, doi:10.1016/j.jvolgeores.2014.05.010.

Mauriello, P., and Patella, D., 2009, A data-adaptive probability-based fast ERT inversion method: Progress In Electromagnetics Research, v. 97, p. 275-290, doi: 10.2528/10.2528/.

Németh, K., 2010, Volcanic glass textures, shape characteristics and compositions of phreatomagmatic rock units from the Western Hungarian monogenetic volcanic fields and their implications for magma fragmentation, Central Europe: Journal of Geoscience, v. 2, p. 399–419, doi: 10.2478/v10085-010-0015-6

Neri, A., Bevilacqua, A., Esposti Ongaro, T., Isaia, R., Aspinall ,W.P., Bisson, M., Flandoli, F., Baxter, P.J., Bertagnini, A. Iannuzzi, E., Orsucci, S., Pistolesi, M., Rosi, M., and Vitale, S., 2015, Quantifying volcanic hazard at Campi Flegrei caldera (Italy) with uncertainty assessment: II. Pyroclastic density current invasion maps, Journal of Geophysical Research - Solid Earth, in press.

Orsi, G., Civetta, L., Del Gaudio, C., De Vita, S., Di Vito, M.A., Isaia, R., Petrazzuoli, S., Ricciardi, G.P., and Ricco, C., 1999, Short-term ground deformations and seismicity in the nested

Campi Flegrei caldera (Italy): Journal of Volcanology and Geothermal Research, v. 91,p. 415−451.

Orsi, G., Di Vito, M.A., and Isaia, R., 2004, Volcanic hazard assessment at the restless Campi Flegrei caldera: Bullettin of Volcanology, v. 66, p. 514–530, doi: 10.1007/s00445-003-0336-4.

Pardo, N., Macias, J.L., Giordano, G., Cianfarra, P., Bellatreccia, F., and Avellán, D.R., 2009. The ~1245 yr BP Asososca maar eruption: the youngest event along the Nejapa-Miraflores volcanic fault, western Managua, Nicaragua: Journal of Volcanology and Geothermal Research, v. 184, p. 292-312

Pardo, N., Cronin, S.J., Nemeth, K., Brenna, M., Schipper, C.I., Breard, E., White, J.D.L., Procter, J., Stewart, B., Agustin-Flores, J., Moebis, A., Zernack, A., Kereszturi, G., Lube, G., Auer, A., Neall, V., and Wallace, C., 2014, Perils in distinguishing phreatic from phreatomagmatic ash; insights into the eruption mechanisms of the 6 August 2013 Mt Tongariro eruption: Journal of Volcanology and Geothermal Research, v. 286, p. 397–414, doi: 10.1016/j.jvolgeores.2014.07.002.

Park, S.K., and Van, G.P., 1991, Inversion of pole-pole data for 3D resistivity structure beneath arrays of electrodes: Geophysics, v. 56, p. 951-960, doi: 10.1190/1.1443128.

Petrosino, S., Damiano, N., Cusano, P., Di Vito, M. A., de Vita, S. and Del Pezzo, E., 2012, Subsurface structure of the Solfatara volcano (Campi Flegrei caldera, Italy) as deduced from joint seismic-noise array, volcanological and morphostructural analysis: Geochemestry Geophysical Geosystems, v. 13, Q07006, doi:10.1029/2011GC004030.

Piochi, M., Kilburn, C., Di Vito, M.A., Mormone, A., Tramelli, A., Troise, C., and De Natale, G., 2014, The volcanic and geothermally active campi flegrei caldera: an integrated multidisciplinary image of its buried structure: International Journal of Earth Sciences, v. 103, p. 401-421, doi:10.1007/s00531-013-0972-7.

Ross, P.-S. and White, J.D.L., 2006. Debris jets in continental phreatomagmatic volcanoes: A field study of their subterranean deposits in the Coombs Hills vent complex, Antarctica: Journal of Volcanology and Geothermal Research, v. 149, p. 62–84, doi:10.1016/j.jvolgeores.2005.06.007.

Ross, P.-S., White, J.D.L., Zimanowski, B. and Büttner, R., 2008a, Multiphase flow above explosion sites in debris-filled volcanic vents: Insights from analogue experiments: Journal of Volcanology and Geothermal Research, v. 178, p. 104–112, doi:10.1016/j.jvolgeores.2008.01.013.

Ross, P.-S., White, J.D.L., Zimanowski, B. and R. Büttner, 2008b, Rapid injection of particles and gas into non-fluidized granular material, and some volcanological implications: Bullettin of Volcanology, v. 70, p. 1151–1168, doi:10.1007/s00445-008-0230-1.

Ross, P.-S., Delpit, S., Haller, M.J., Németh, K. and Corbella, H., 2011, Influence of the substrate on maar-diatreme volcanoes—An example of a mixed setting from the Pali Aike volcanic field, Argentina: Journal of Volcanology and Geothermal Research, v. 201, p. 253–271, doi:10.1016/j.jvolgeores.2010.07.018.

Sasaki, Y., 1994, 3D resistivity inversion using the finite-element method: Geophysics, v. 59, p. 1839-1848, doi: 10.1190/1.1443571.

Scandone, R., D’Amato, J. and Giacomelli, L., 2010, The relevance of the 1198 eruption of Solfatara in the Phlegraean Fields (Campi Flegrei) as revealed by medieval manuscripts and historical sources: Journal of Volcanology and Geothermal Research, v. 189, p. 202–206, doi:10.1016/j.jvolgeores.2009.09.012.

Self, S., Kienle, J. and Huot, J.-P., 1980, Ukinrek Maars, Alaska, II. Deposits and formations of the 1977 craters: Journal of Volcanology and Geothermal Research, v. 7, p. 39–65.

Scott, B.J., and Potter, S.H., 2014, Aspects of historical eruptive activity and volcanic unrest at Mt. Tongariro, New Zealand: 1846–2013, Journal of Volcanology and Geothermal Research, v. 286, p. 263–276, doi:10.1016/j.jvolgeores.2014.04.003.

Shima, H., 1990, Two-dimensional automatic resistivity inversion technique using alpha centers: Geophysics, v. 55, p. 682-694, doi: 10.1190/1.1442880

Smith, V.C., Isaia, R., and Pearce, N.J.G., 2011, Tephrostratigraphy and glass compositions of post-15 kyr Campi Flegrei eruptions: implications for eruption history and chronostratigraphic markers: Quaternary Science Reviews, v. 30, p. 3638-3660, doi: 10.1016/j.quascirev.2011.07.012.

Son, M., Kim, J.S., Jung Ki, J.S., Kim, M.-C. and Sohn, Y.K., 2012, Tectonically controlled vent migration during maar-diatreme formation: An example from a Miocene half-graben basin in SE Korea: Journal of Volcanology and Geothermal Research, v. 223-224, p. 29–46, doi:10.1016/j.jvolgeores.2012.02.002.

Sottili, G., Palladino, D. M., Gaeta, M., and Masotta, M., 2012, Origins and energetics of maar volcanoes: Examples from the ultrapotassic Sabatini Volcanic District (Roman Province, Central Italy): Bullettin of Volcanology, v. 74, p. 163–186, doi:10.1007/s00445-011-0506-8.

Tamas, C. G., and Milési, J.P., 2002, Hydrovolcanic breccia pipe structures - general features and genetic criteria – 1. Phreatomagmatic breccias: Studia Universitatis Babe-Bolyai, Geologia, vol. XLVII, 1, p. 127-147.

Todesco, M., Chiodini, G., and Macedonio, G., 2003. Monitoring and modelling hydrothermal fluid emission at La Solfatara (Phlegrean Fields, Italy). An interdisciplinary approach to the study of diffuse degassing: Journal of Volcanology and Geothermal Research, 125,1-2, 57-79.

Tripp, A.C., Hohmann, G.W., and Swift, C.M.Jr., 1984, Two-dimensional resistivity inversion: Geophysics, v. 49, p. 1708-1717, doi: 10.1190/1.1441578.

Troiano, A., Di Giuseppe, M.G., Patella, D., Troise, C., and De Natale, G., 2014, Electromagnetic outline of the Solfatara-Pisciarelli hydrothermal system, Campi Flegrei (Southern Italy): Journal of Volcanology and Geothermal Research, v. 277, p. 9-21, doi: 10.1016/j.jvolgeores.2014.03.005

Valentine, G.A., 2012, Shallow plumbing systems for small-volume basaltic volcanoes, 2: Evidence from crustal xenoliths at scoria cones and maars: Journal of Volcanology and Geothermal Research, v. 223–224, p. 47–63, doi:10.1016/j.jvolgeores.2012.01.012.

Valentine, G.A., and White, J.D.L., 2012, Revised conceptual model for maar-diatremes: Subsurface processes, energetics, and eruptive products: Geology, v. 40, p. 1111–1114, doi:10.1130/G33411.1.

Valentine, G.A., Shufelt, N.L. and Hintz, A.R.L., 2011, Models of maar volcanoes, Lunar Crater (Nevada, USA): Bulettin of Volcanology, v. 73, p. 753–765, doi:10.1007/s00445-011-0451-6.

Vilardo, G., Isaia, R., Ventura, G., De Martino, P., and Terranova, C., 2010, InSAR Permanent Scatterer analysis reveals fault reactivation during inflation and deflation episodes at Campi Flegrei caldera: Remote Sensing of Environment, v. 114, p. 2373-2383, doi:10.1016/j.rse.2010.05.014

Vitale, S., and Isaia, R., 2014, Fractures and faults in volcanic rocks (Campi Flegrei, southern Italy): insight into volcano-tectonic processes: International Journal of Earth Science, v. 103, p. 801-819, doi: 10.1007/s00531-013-0979-0

Ward, S.H., 1990. Resistivity and induced polarization methods. In Geotechnical and Environmental Geophysics, Vol. I: Review and Tutorials (ed. S.H. Ward), 147-189. Investigations in Geophysics No.5, SEG, Tulsa.

White, J.D.L., 1991, Maar-diatreme phreatomagmatism at Hopi Buttes, Navajo Nation (Arizona), USA: Bulletin of Volcanology, v. 53, p. 239–258.

White, J.D.L., and Ross P.S., 2011, Maar-diatreme volcanoes: A review: Journal of Volcanology and Geothermal Research, v. 201, p. 1–29, doi:10.1016/j.jvolgeores.2011.01.010.

Zeyen, H., Pessel, M., Ledésert, B., Hébert, R., Bartier, D., Sabin, M., and Lallemant, S., 2011, 3D electrical resistivity imaging of the near-surface structure of mud-volcano vents: Tectonophysics, v. 509, p. 181-190, doi: 10.1016/j.tecto.2011.05.007.

Figure captions

Fig. 1. Geological map of Campi Flegrei (from Vitale and Isaia, 2014, modified).

Fig. 2. Vent location within the central sector of the Campi Flegrei caldera and chronostratigraphy between 5.6 ka and 1538 AP (from Isaia et al., 2009, modified).

Fig.3. (a) Geological map of the Solfatara area.

Fig.4. Stratigraphic logs, simplified stratigraphic scheme and map of log measurements.

Fig. 5. NE corner of Solfatara volcano: (a) Sharp contact between pipe breccias and AMS deposits (host rock). (b) Centimeter sized accretionary lapilli in the injection breccias. (c) Highly deformed host rock along the contact with the breccias. (d) Panoramic view of the Solfatara cryptodome and paleosol pictures. (e) Particular of the contact between the cryptodome and the pre-AMS deposits, marked by almost vertical fault and dragged layering. (f) low-altered lava of cryptodome showing elongated sanidine crystals.

Fig. 6. (a) Distribution map of Solfatara deposits in the CF caldera. (b) Proximal deposits of Solfatara (SE rim of Solfatara crater). (c) Varved lacustrine deposits with carbonized wood (SE corner of Solfatara crater).

Fig. 7. (a) Ring fault of AMS caldera sealed by the Solfatara deposits (Pisciarelli). (b) NE-SW normal fault in pre-AMS/and AMS deposits sealed by Solfatara deposits (Pisciarelli). (c) Mud pools

and fumaroles localized along the NE continuation of the fault shown in the previous picture (Pisciarelli). (d) Secondary ring normal faults and related damage zone (Solfatara). (e) Particular of ring fault-related damage zone (Solfatara). (f) Collapse breccias and damage zone in the wall rock (Solfatara). (g) Particular of collapse breccias showing large blocks of wall rocks (AMS deposits).

Fig.8. (a) Upward convex fault and related fault bend fractures in pre-AMS deposits (Solfatara). (b) About orthogonal sets of fractures in recent deposits (Solfatara). (c) Three sets of fractures in pre-AMS deposits (Pisciarelli). (d) Fracture in recent deposits parallel to the NE-SW fumarole lineament bounding the northern edge of Mt. Olibano (Solfatara). (e) Minor faults related to a main collapse fault in AMS deposits sealed by Solfatara deposits (Solfatara). (f) Steep normal fault in AMS deposits (Solfatara). (h) Minor normal faults in Astroni deposits (Solfatara). (i) Book shelf structure in recent deposits (Solfatara).

Fig. 9. Stereographic projections and contour plots of fracture (a, c, e, g, i, k, m) and fault plane (o) poles (lower hemisphere, Equiareal net). Rose-diagrams of fracture (b, d, f, h, i, l, n) and fault plane (p) directions and dip angles. Frequency histograms: (q) fracture dip angles; (r) normal fault dip angles and (s) normal fault separations.

Fig. 10. (a) S3-vector and T-axis direction map (from this study) and contours of CO_2 Flux in December 1998 (from Todesco et al., 2003). Contour plots of (b) T-axis and (c) S3-vector.

Fig. 11. Fracture density along scan lines (a) SL1; (b) SL2; (c) SL3 and (d) SL4. Stereographic projections, contour plots and rose-diagrams of fractures (lower hemisphere, equiareal net) along the scan lines (e-j) SL1; (k-i) SL2; (m-n) SL3 and (o-p) SL4.

Fig. 12. (a)-(c) ERT profiles. (b)-(d) Geological cross sections (2x vertical exaggeration).

Fig. 13. (a) Schematic model showing the Solfatara diatreme structure along a N-S section (after White and Ross, 2001, modified). (b) Resistivity model E-W section (after Troiano et al., 2014, modified).

Appendix

Electrical Resistivity Tomography

Electrical and electromagnetic methods are among the most suitable tools in volcano-geothermal areas for the subsurface investigations (e.g., Di Maio et al., 1997; 1998; Legaz et al., 2009; Zeyen et al., 2011; Fikos et al., 2012). The resistivity parameter has a large variability and allows the majority of buried structures of volcanological and geothermal interest to be distinguished. To enhance the resolution, the Electrical Resistivity Tomography (ERT) approach is used, which can handle large datasets, now quickly collected by modern computer-assisted, multichannel resistivity meters. Moreover, refined 2D and 3D inversion codes (e.g., Tripp et al., 1984; Shima, 1990; Park and Van, 1991; Li and Oldenburg, 1992; Sasaki, 1994; Loke and Barker, 1995; Dahlin and Zhou, 2004; Mauriello and Patella, 2009) make of ERT invaluable for imaging of volcanic structures down to a few hundred meters depth. The ERT profiles have been generated for the Solfatara crater by a dipole-dipole configuration. The dipole-dipole source-receiver coupling was chosen as it is compact and sensitive to both lateral location and depth of anomalous source bodies (Ward 1990). The IRIS Syscal Pro system was used as a source, with maximum output voltage and current of 800 V and 2 A, respectively, and a full array of maximum 72 electrodes. The ERT lines have singularly been inverted using the RES2DINV commercial software (Loke, 2012; Loke and Barker, 1996), including topography. Taking into account the rough volcanic environment in which the data were acquired, the average RMS associated uncertainty of ~7 was considered satisfactory.

Figure1

Click here to download high resolution image

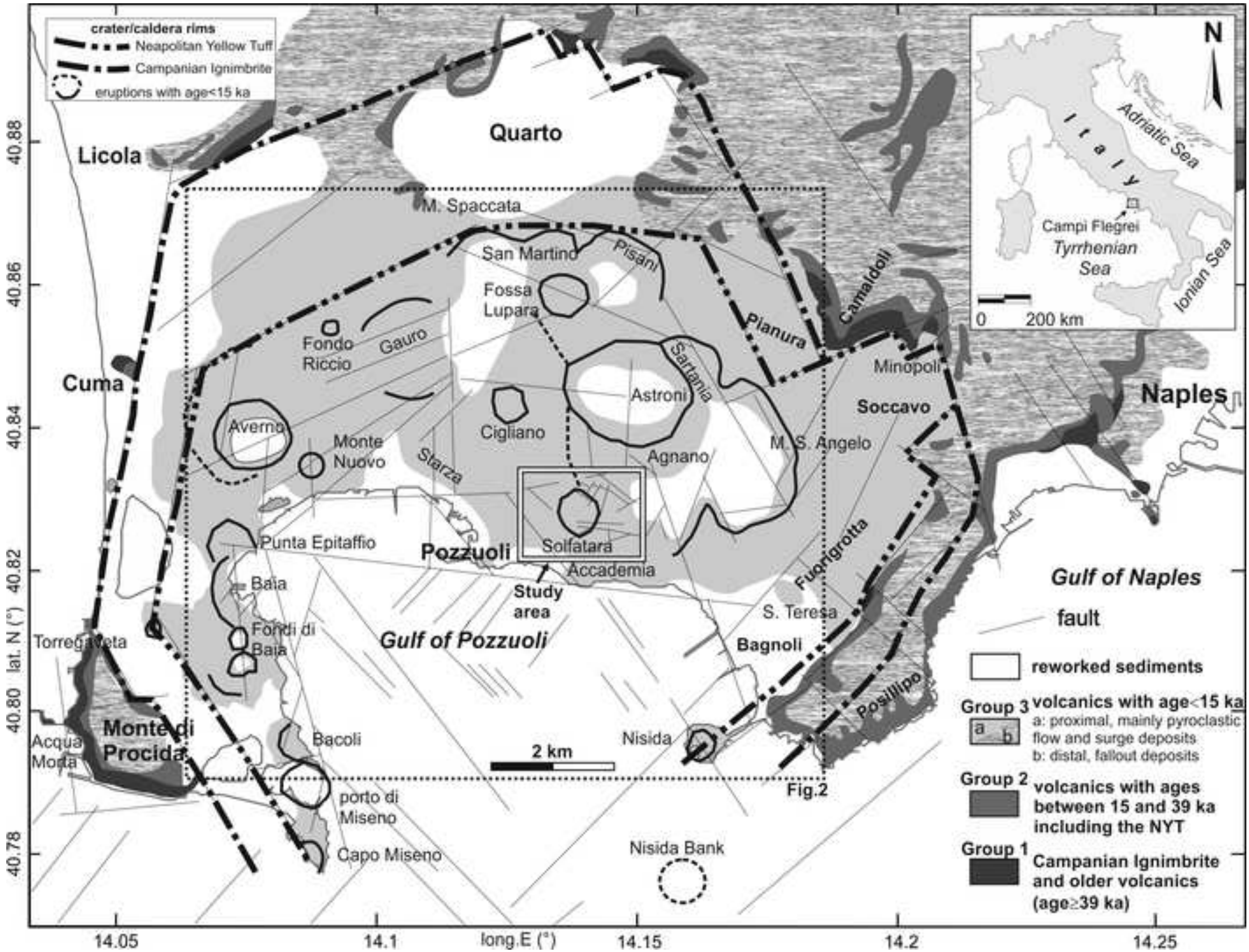

Figure2

Click here to download high resolution image

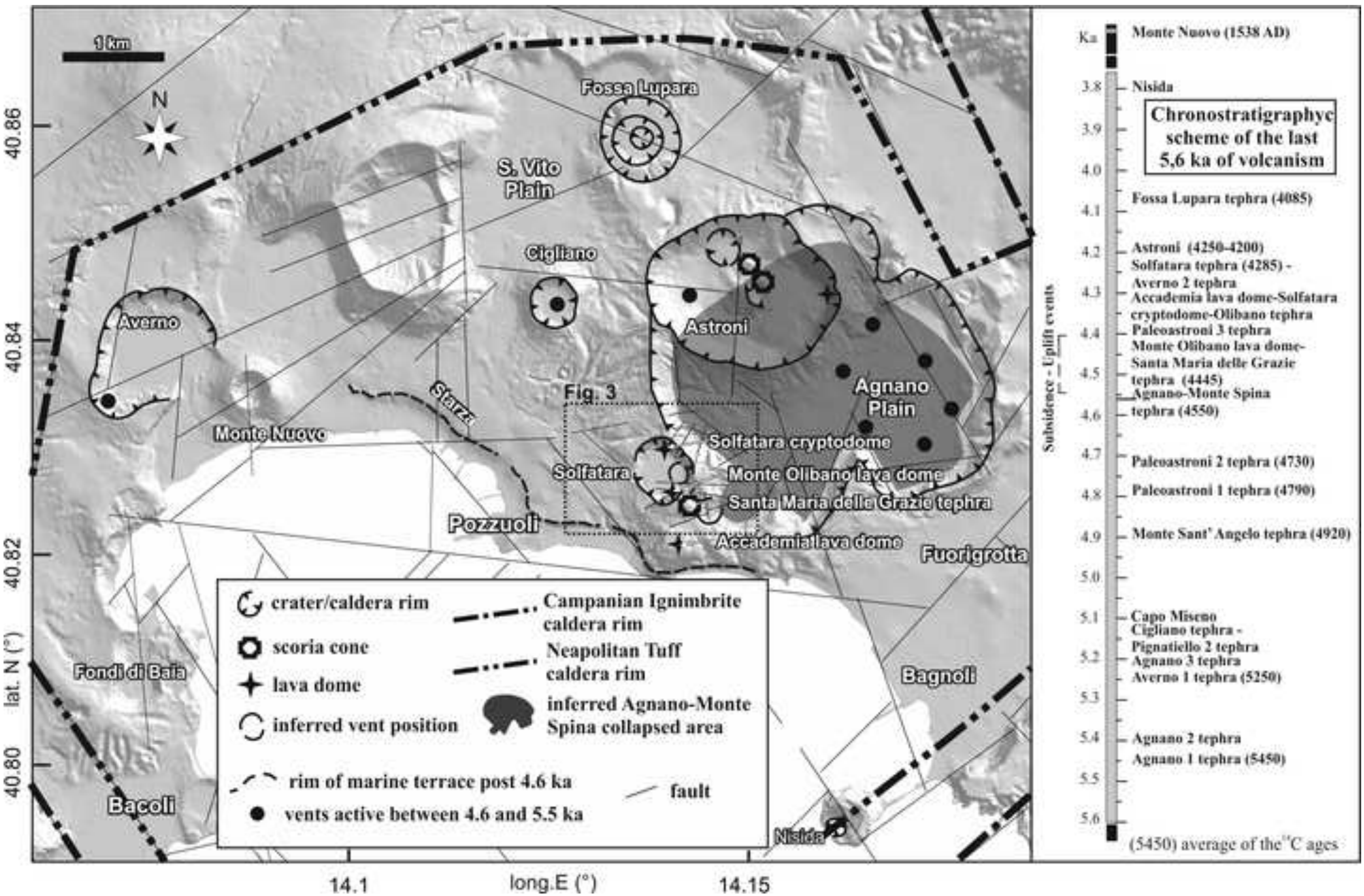

Figure3
Click here to download high resolution image

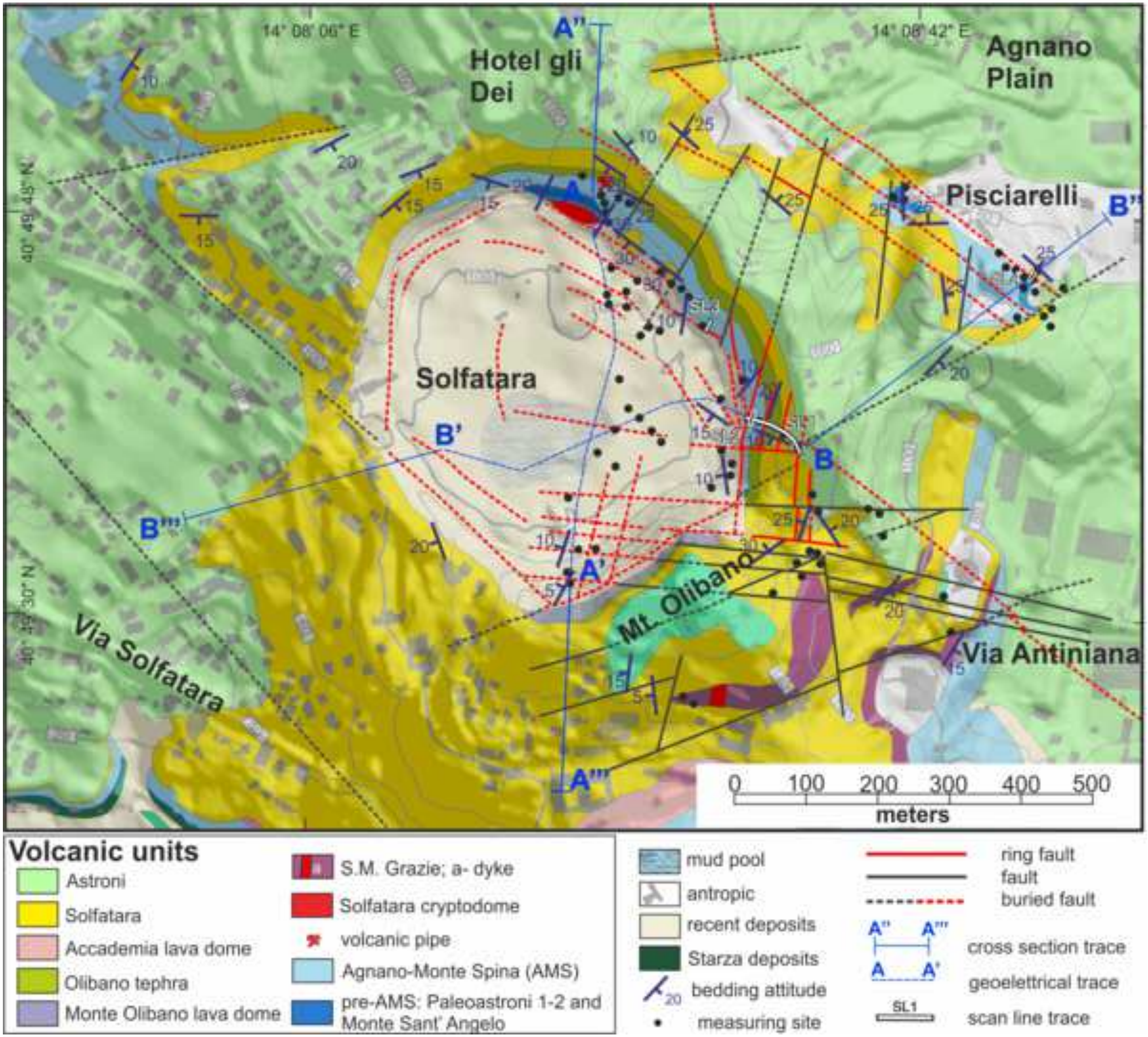

Figure4
Click here to download high resolution image

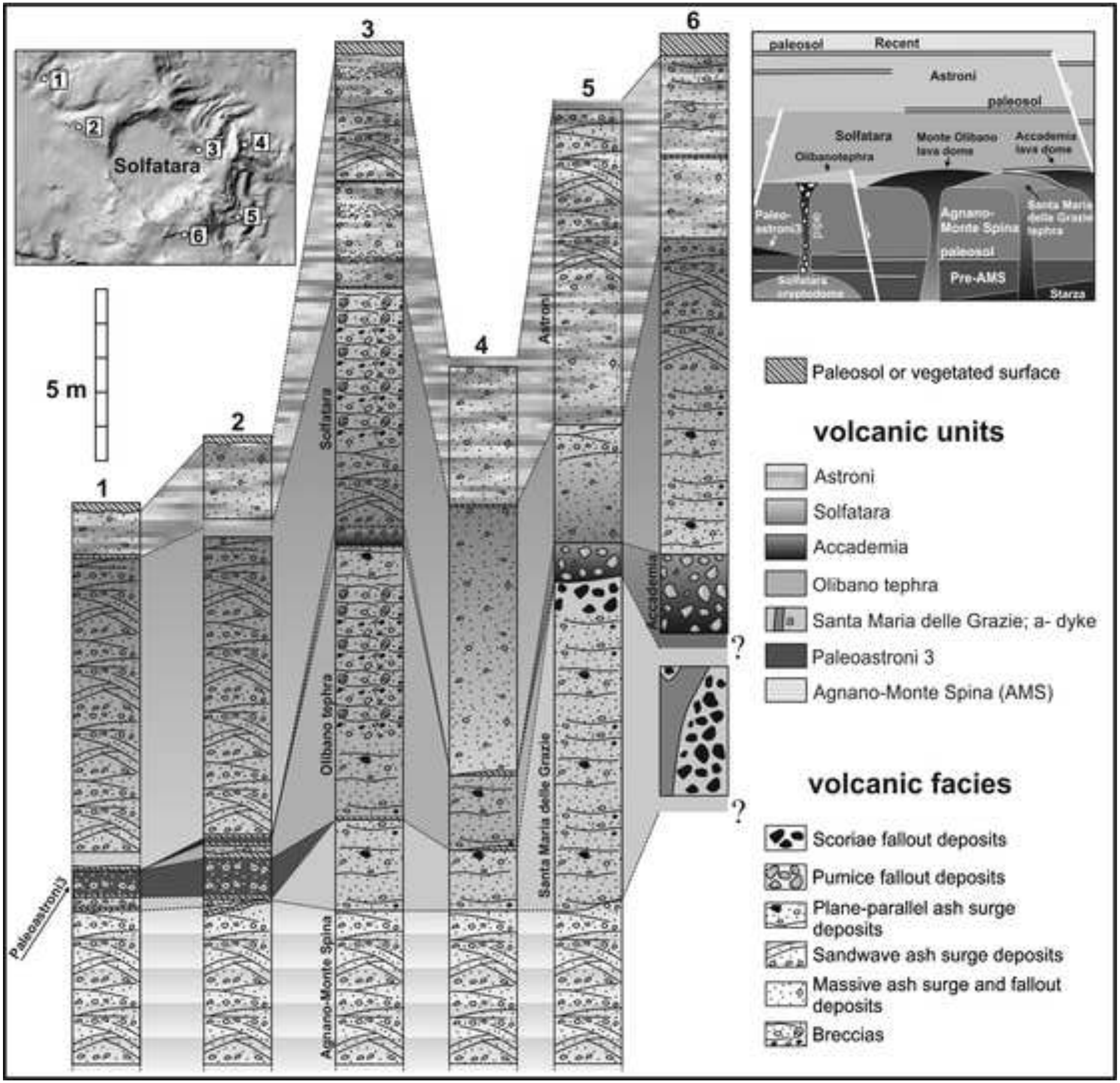

Figure5
Click here to download high resolution image

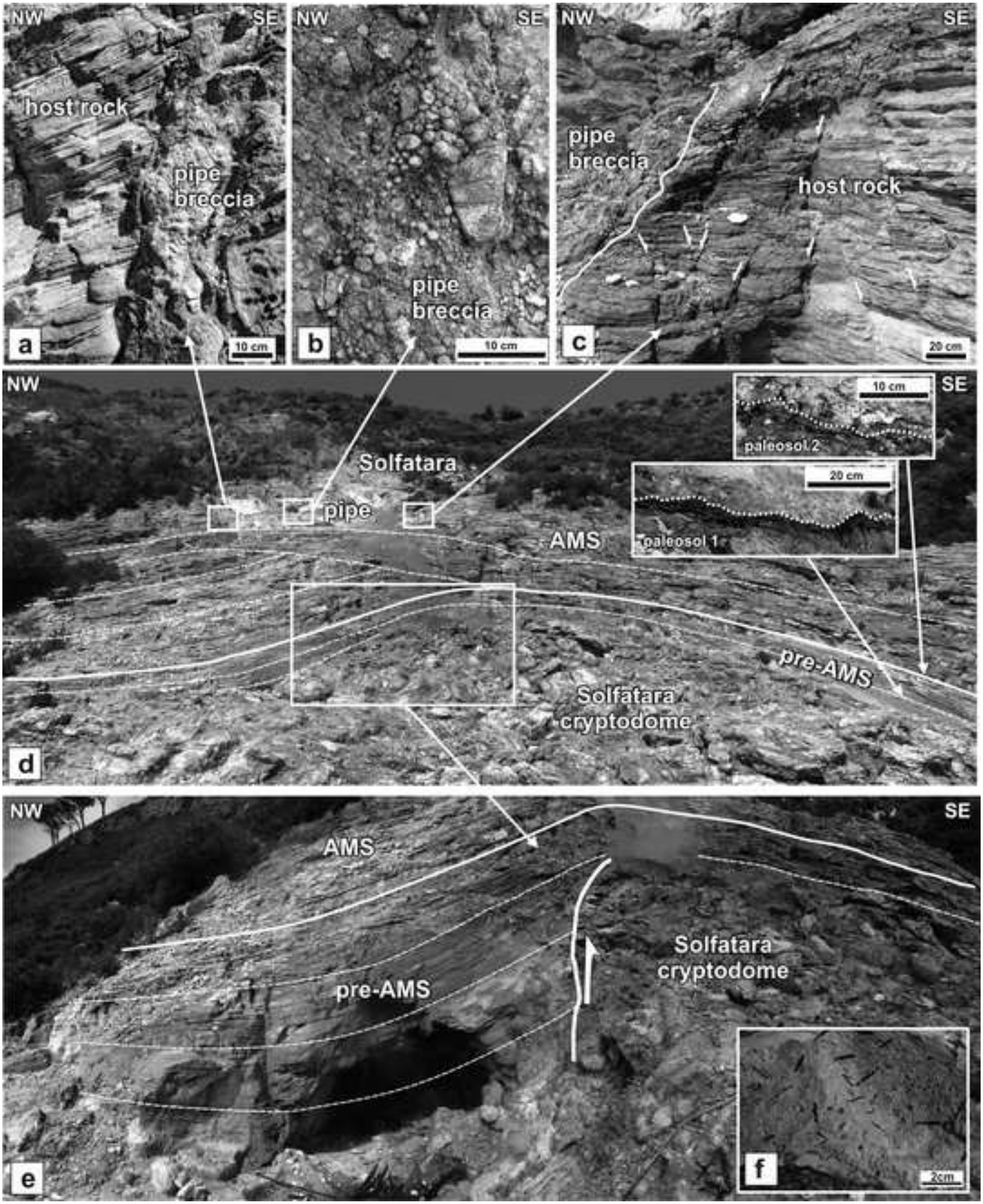

Figure6

Click here to download high resolution image

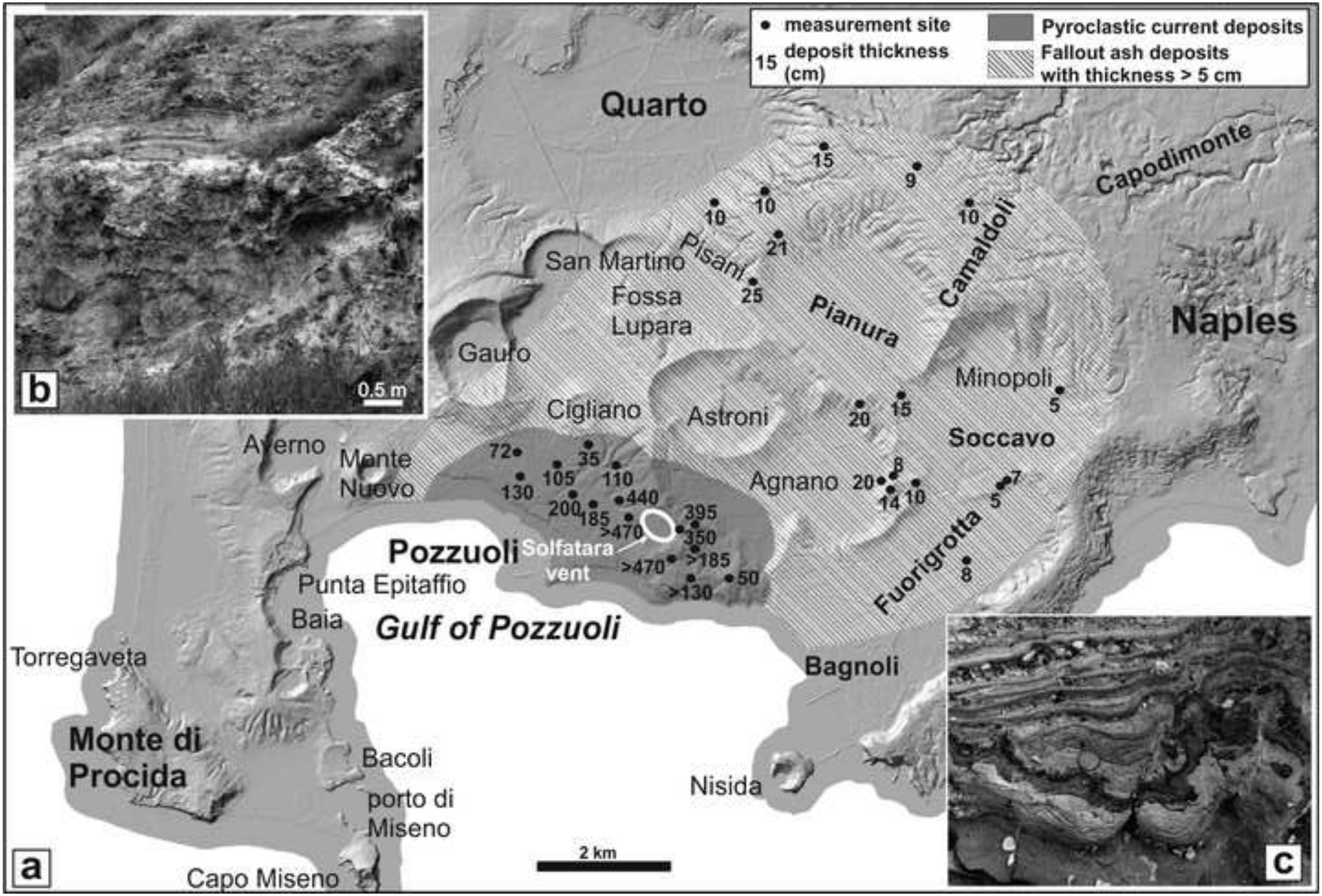

Figure7

Click here to download high resolution image

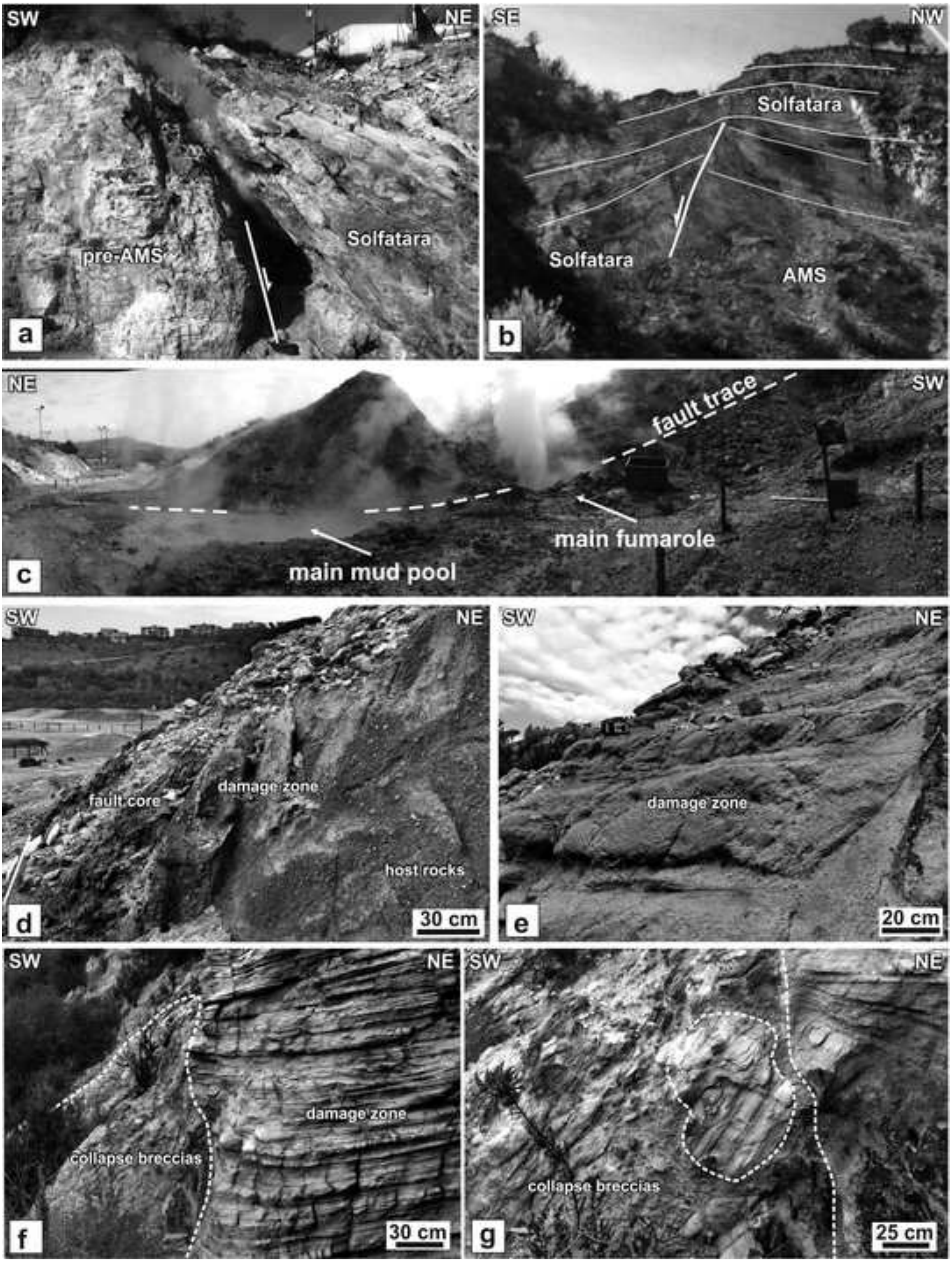

Figure8

Click here to download high resolution image

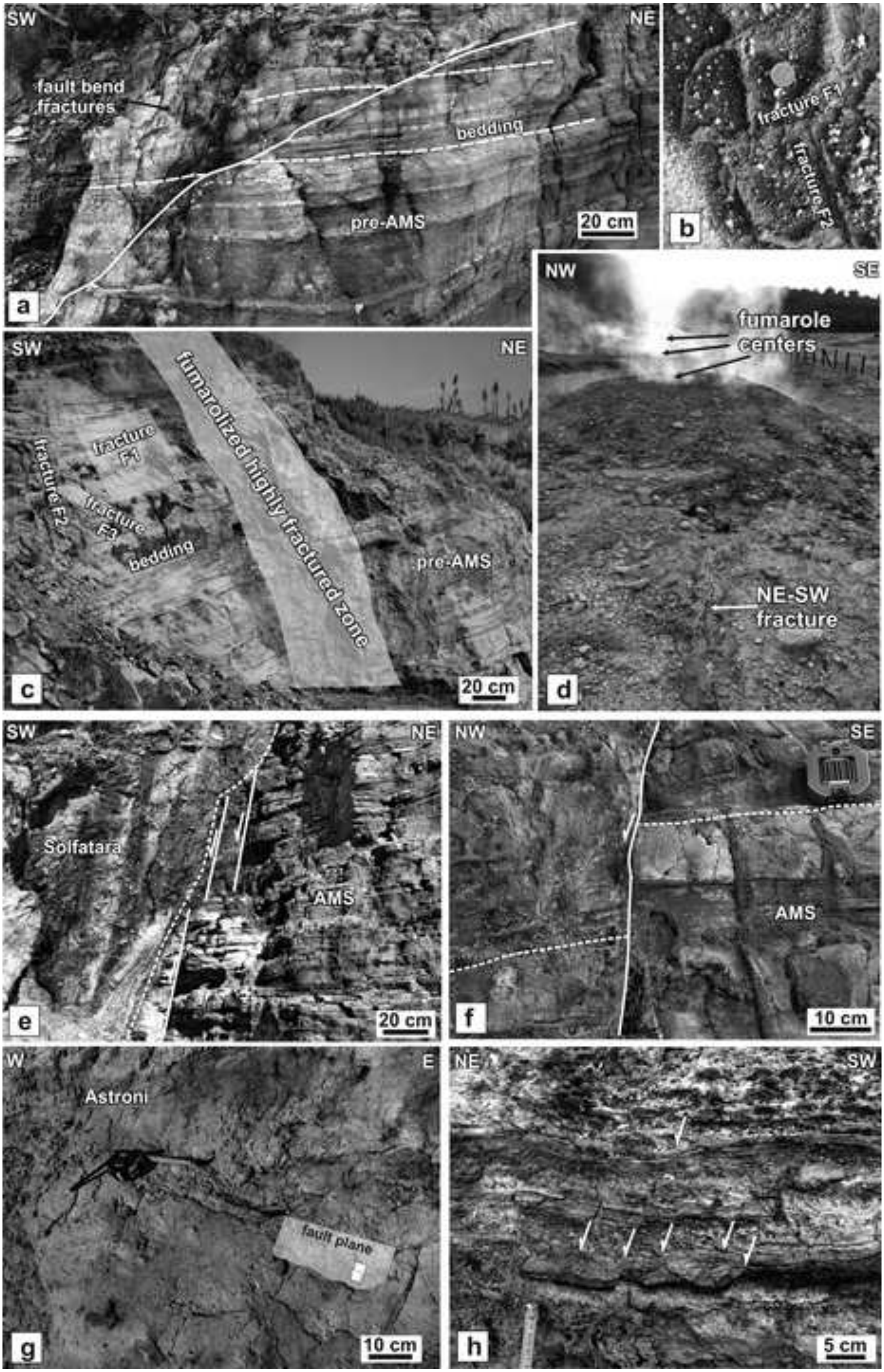

Figure9

Click here to download high resolution image

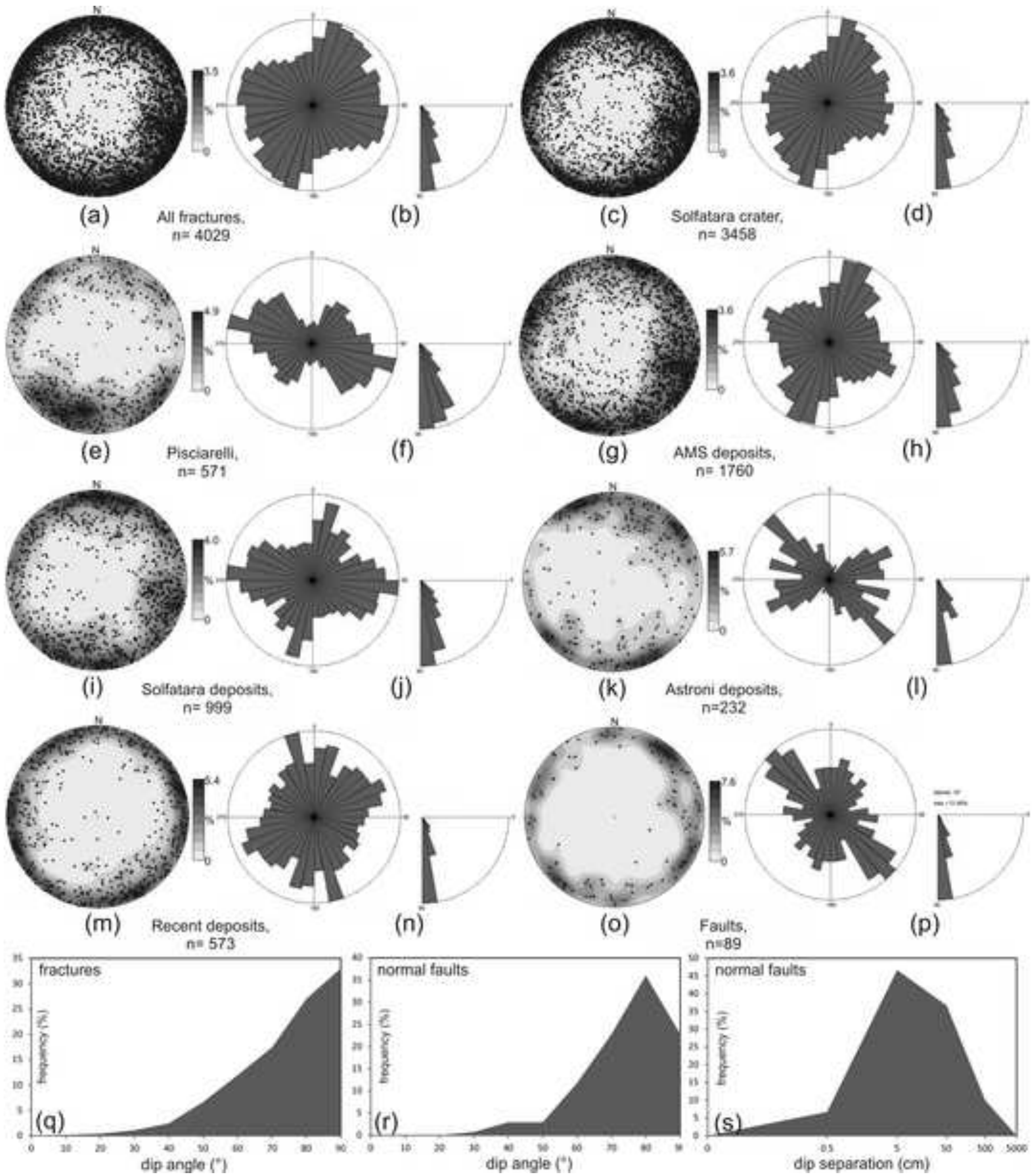

Figure10
Click here to download high resolution image

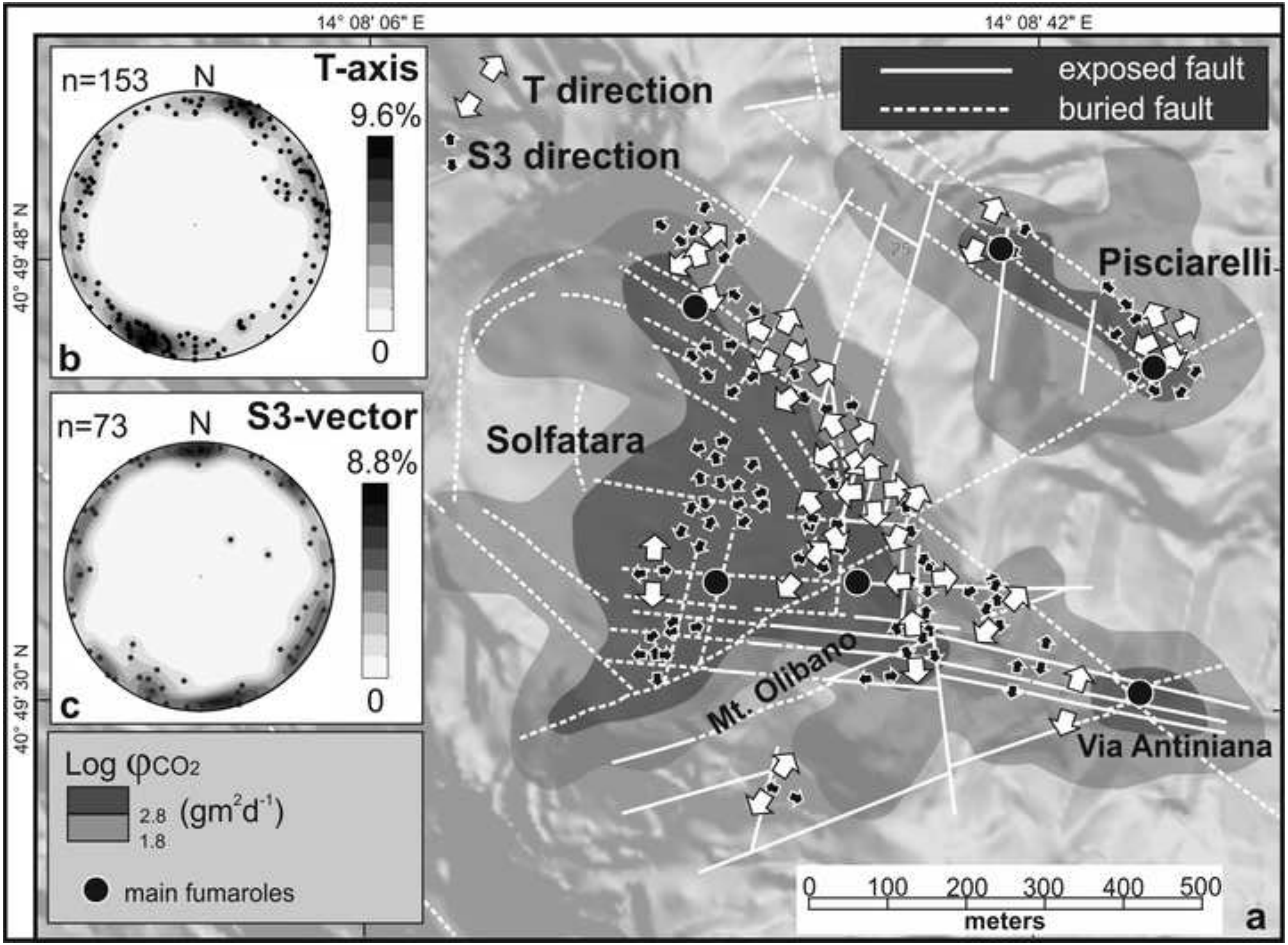

Figure11
Click here to download high resolution image

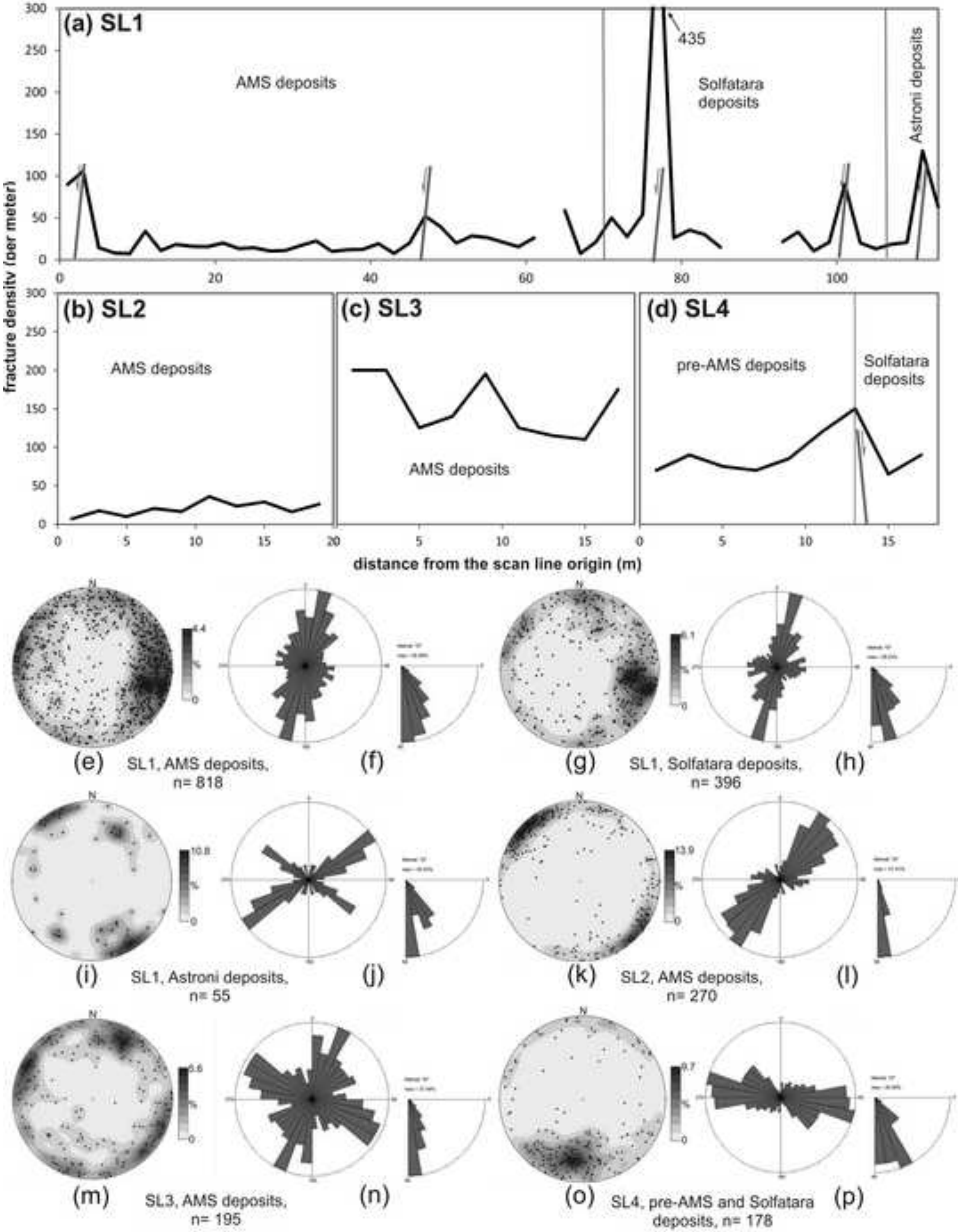

Figure12
Click here to download high resolution image

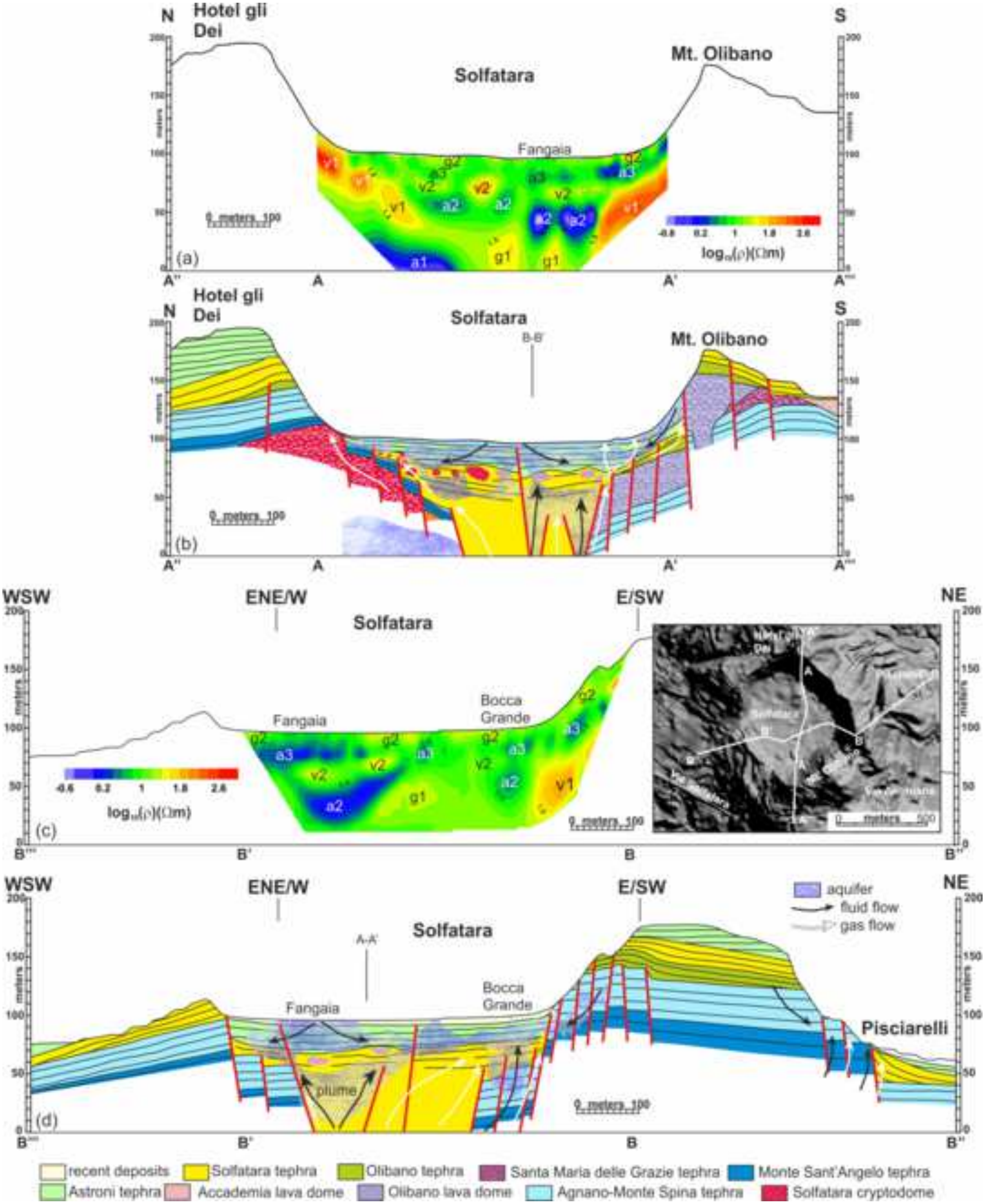

Figure13

Click here to download high resolution image